Advances in Colloid and Interface Science 299 (2022) 102578

Contents lists available at ScienceDirect

Advances in Colloid and Interface Science

journal homepage: www.elsevier.com/locate/cis

Historical Perspective

Metallic core-shell nanoparticles for conductive coatings and printing

Anna Pajor-Świerzy [a,*], Krzysztof Szczepanowicz [a], Alexander Kamyshny [b], Shlomo Magdassi [b,*]

[a] Jerzy Haber Institute of Catalysis and Surface Chemistry, Polish Academy of Sciences, Niezapominajek 8, 30-239 Kraków, Poland
[b] Casali Center for Applied Chemistry, Institute of Chemistry and the Center for Nanoscience and Nanotechnology, The Hebrew University of Jerusalem, Edmond J. Safra Campus, 91904 Jerusalem, Israel

ARTICLE INFO

Keywords:
Metallic core-shell nanoparticles
Synthesis of core-shell nanoparticles
Oxidation stability
Conductive inks
Conductive coatings
Printed electronics

ABSTRACT

The review is focused on bimetallic nanoparticles composed of a core formed by low-cost metal having high electrical conductivity, such as Cu and Ni, and a protective shell composed of stable to oxidation noble metal such as Ag or Au. We present the chemical and physical approaches for synthesis of such particles, as well as the combination of the two, the stability to oxidation of core-shell nanoparticles at various conditions, and the formulation of conductive compositions and their application in conductive coatings and printed electronics.

1. Introduction

In recent years, printed electronics, i.e. application of 2D and 3D coating and printing technologies for the fabrication of various 2D and 3D electronic devices, has acquired great interest and is a successfully growing field of materials science and technology [1–8]. The applications span from electrical circuits, transparent conductive films, thin-film transistors, solar cells, RFID tags, flexible touch panels and light-emitting displays, electrochemical storage devices, supercapacitors, to electrical actuators. Among noncontact techniques are inkjet printing, electrohydrodynamic, and aerosol jet printings which are often used [1,2,6–12], while screen, gravure, and flexographic printings are examples of contact-based techniques [1,5,13–16]. In addition, conductive patterning can be performed by electroless plating, drop-casting, dip-coating, spray-coating, bar(rod)-coating, spin-coating, thermal nano-imprint lithography, vacuum filtration followed by film transfer, or transferring from an etched substrate, and by electrophoretic deposition followed by hot pressing transfer [5,14,17–24]. Each of these techniques has advantages and disadvantages, and the patterning method is usually determined by the features of the functional material and ink formulation to be deposited, as well as by the substrate characteristics and the required properties of fabricated devices.

The functional material to be used for conductive coatings may be metal nanoparticles (NPs) and nanowires (NWs) [2,5,25–27], carbon nanotubes (CNTs), both single-walled (SWCNT) and multi-walled (MWCNT) [2,5,25,28–30], graphene sheets [2,5,25,28,29], conductive polymers (dissolved or dispersed) [28–30] as well as organometallic compounds and complexes as precursors, which convert to metal upon post-printing treatment [2,5,26,31–34].

The selection of the conductive material is usually determined by the required performance of the fabricated device. For example, if optical transparency is an important parameter, thin films or grids of conductive material should be deposited on a proper substrate [5,35]. Excellent materials for obtaining transparent conductors are Ag and Cu NWs [19,27,35,36]. Because of the superior mechanical properties of individual CNTs, thin films made of randomly distributed CNTs show excellent mechanical performance such as flexibility, stretchability, and foldability that makes them together with metal NWs an effective material for the fabrication of flexible electronic devices [5].

However, one of the most important characteristics of such coatings is their conductivity. The highest conductivity is usually obtained while using metallic NPs and NWs. Highly conductive metals which are stable to oxidation, such as silver ($\sigma = 6.3 \times 10^7\ \Omega^{-1}\ m^{-1}$) and gold ($\sigma = 4.42 \times 10^7\ \Omega^{-1}\ m^{-1}$) are the best for utilization in conductive inks, and currently silver is the most widely used material. At optimal conditions, including proper post-printing sintering process, the conductivity of coatings obtained with the use of Ag NPs is comparable with the conductivity of bulk metal [2,5]. For example, the conductivity of silver tracks deposited on PEN (polyethylene naphthalate) substrate was as high as 40% and 60% of that for bulk silver after the combination of photonic and microwave or plasma and microwave sintering, respectively [37,38]. However, due to the high cost of silver and other noble

* Corresponding authors.
E-mail addresses: anna.pajor-swierzy@ikifp.edu.pl (A. Pajor-Świerzy), magdassi@mail.huji.ac.il (S. Magdassi).

https://doi.org/10.1016/j.cis.2021.102578
Received 7 October 2021; Received in revised form 22 November 2021; Accepted 23 November 2021
Available online 26 November 2021
0001-8686/© 2021 The Authors. Published by Elsevier B.V. This is an open access article under the CC BY license (http://creativecommons.org/licenses/by/4.0/).

metals, a major challenge in this field is to replace them with cheaper ones, such as copper ($\sigma = 5.96 \times 10^7\ \Omega^{-1}\ m^{-1}$), aluminum ($\sigma = 3.78 \times 10^7\ \Omega^{-1}\ m^{-1}$) or nickel ($\sigma = 1.43 \times 10^7\ \Omega^{-1}\ m^{-1}$). This would depend on the success in avoiding oxidation of these metals under ambient conditions, otherwise an inert atmosphere would be required during the fabrication and coating processes [2,31,39,40]. For example, aluminum undergoes rapid oxidation in the air forming a dense thin amorphous Al_2O_3 layer with a thickness of 2–6 nm [41,42], that results in the loss of electrical conductivity and makes aluminum NPs inapplicable for conductive ink formulations. Oxidation of copper NPs is less rapid as compared with aluminum, especially in the presence of an excess of a reducing agent [43]. Protected copper NPs can be obtained by coating the individual particles with a dense layer of capping agent (such as alkanethiols, long chain carboxylic acids, surfactants and polymers) [40,44–46]. However, this approach does not result in long-term stability but only in minimization of oxygen penetration to the metal NPs and retarding their oxidation. In this respect, the best method is the deposition of a layer of a noble metal, which forms a protective shell on the surface of oxidizable metallic NP i.e. synthesis of core-shell NPs (hereinafter, $M_{core}@M_{shell}$).

There are numerous reports on the synthesis of various core-shell NPs: Pd@Ag, Pd@Pt, Ag@Au, Au@Ag, Ag@Pt, Au@Pd, Ru@Pt, Co@Pt, [2,47–49]. Many of such NPs are characterized by enhanced catalytic or photocatalytic performance, unique optical properties as well as by antibacterial activity [49–51]. However, to the best of our knowledge, there is no review, which summarizes the synthesis and properties of low-cost metallic core-shell NPs to be applied for conductive coatings and printed electronics.

Therefore, in this review we focused on bimetallic nanoparticles composed of core formed by high-conductivity, low-cost metals, such as Cu and Ni, and stable to oxidation protective shell formed by a noble metal such as Ag or Au [40,43,52–58]. We will describe the methods for their synthesis, stability to oxidation, formulation of conductive compositions and their application in conductive coatings and printed electronics.

2. Synthesis of metallic NPs (general overview)

Conventionally, metal NPs, both noble and non-noble, are formed by breaking the bulk metal into small particles (top-down approach) or by reaction of a metal precursor (ions or molecules) with a proper reducing agent as well as by decomposition of precursors such as salts and organometallic molecules (bottom-up approach).

Top-down methods include mechanical grinding, laser ablation in a proper liquid, electro-explosion of a metal wire followed by condensation of metal vapors, plasma excitation of metal plates, powders, or wires followed by transport of the formed NPs with a stream of inert gas into a proper liquid or onto a solid substrate [2,5,57–61].

The bottom-up approach is mainly based on “wet” chemical processes, and the liquid medium can vary from water to polar and nonpolar solvents, polyols, and also ionic liquids [62–65]. As to precursor decomposition, several metal salts and organometallic compounds (such as carbonyldibenzylidene acetonates, acetyl acetonates, formates, complexes of metals with fatty acids) can decompose either spontaneously upon heating, or in the presence of a reducing agent, e.g. gaseous hydrogen, with the formation of metal NPs [31,33,34,66–69].

Wet chemistry methods yield a great variety of dispersions with various particle characteristics such as size distribution, morphology, stability towards aggregation and sedimentation, etc. These are controlled by tailoring the experimental parameters of the reaction, such as concentration of reagents, redox potentials of the reducing agent, temperature, pH, rate of reagent addition, the presence of pre-formed seeds, type and concentration of protective agents [62,70–73].

The first step in the formation of metal NPs in liquid from the corresponding ions is their reduction to metal atoms. The reaction is possible only if the reduction potential of the reducing agent is more negative than the reduction potential of the metal precursor. In aqueous medium, cations of strongly electropositive metals, such as Ag^+ ($E^0 = 0.8$ V), Au^{3+} ($E^0 = 1.5$ V), Pt^{2+} ($E^0 = 1.2$ V), and Pd^{2+} ($E^0 = 0.99$ V) [74] can be reduced by relatively mild reducing agents. Cations of moderately electropositive metals, for example, Cu^{2+} ($E^0 = 0.34$ V), require stronger reducing agents, while cations of electronegative metals, such as Ni^{2+} ($E^0 = -0.23$ V), and Sn^{2+} ($E^0 = -0.14$) [74] can be reduced only by strong reducing agents, and the reaction proceeds usually at elevated temperatures [62,75–79].

Among the reducing agents, the most often used are sodium borohydride, $NaBH_4$, and hydrazine, N_2H_4, which are more effective in alkaline medium ($E^0 = -1.24$ V and -1.16 V, respectively), citrate ($E^0 = -0.56$ V), and ascorbic acid [62,74]. Metal ions can also be reduced by organic compounds containing oxidizable hydroxyl and carbonyl groups (alcohols with α-hydrogen, aldehydes, carbohydrates) and organic amines [62,80]. Sodium phosphinate was also used as a reducing agent for the synthesis of metal NPs [81,82].

Reduction of metal ions with the formation of NPs can also be performed by electrolysis of a metal salt in solution [83,84], as well as by sonochemical [85,86] and sonoelectrochemical [87,88] methods. High energy radiations (UV-, γ-, and electron beam) [89–92] and microwave irradiation [93–96] are also applied to obtain dispersions of metal NPs.

To overcome the oxidation problem during the synthesis of easily oxidizable metals, such as Cu, Ni, and Sn, the process is often performed in organic solvents such as polyols [52,63,81,82,94,97,98] and under inert atmosphere (Ar, N_2) [44,46,56,96,99–102].

An important parameter, which determines the application of NP dispersions is their stability to aggregation and precipitation. To prevent these undesirable processes, a stabilizing agent (dispersant) should be added to the reaction mixture. Selecting the proper stabilizer and the composition of the reaction medium are of great importance since these components affect the shelf-life and the overall performance of conductive inks. There are three main mechanism of protective action: (i) electrostatic, providing stabilization of charged molecules due to repulsion of electrical double layers surrounding particles (DLVO theory); (ii) steric, that is achieved by surrounding the particles with a layer of bulky molecules, such as molecules of a surfactant or a polymer mostly of nonionic type, which create a barrier preventing the contact of particles and (iii) electrosteric, that combines both electrostatic and steric mechanisms and is especially effective in aqueous dispersions and water-based ink formulations (an effective electrosteric stabilization can be achieved by using polyelectrolytes). A detailed description of stabilization mechanisms and types of stabilizing agents are presented in [2, 5, and references therein]. We will indicate the specific stabilizing agents while describimg the synthesis of core-shell NPs.

Moreover, as was previously noted, another characteristic of metallic NPs, which is especially important while formulating the inks for conductive coatings and printed electronics is their long-term stability against oxidation. The best approach for the stabilization of easily oxidizable metals is the formation of a conductive protective shell that is stable to oxidation and is composed of a noble metal, i.e. metal-metal core-shell structure.

3. Synthesis of metallic core-shell NPs

In this section, we discuss the current routes that are utilized for the formation of core-shell NPs consisting of noble metal shells (Ag, Au), which protect the cores composed of non-noble NPs (Cu, Ni) and make them suitable for the formulation of cost-effective conductive inks for printed electronics.

Table 1 presents the details of core-shell NPs synthesis to be used for conductive coatings including the main components of the reaction mixtures.

Table 1
Methods of synthesis of core-shell NPs which can be used for conductive coatings.

chemical

	core synthesis			shell synthesis					
Type of NPs/NWs	**Precursor**	**Stabilizer**	**Reducing agent**	**Method**	**Precursor**	**Reducing agent**	**Atmosphere**	**Size [nm]**	**Ref**
Cu@Ag	$CuSO_4$	PVP	glucose ascorbic acid	co-reduction/ one-pot	$[Ag(NH_3)_2]^+$	glucose ascorbic acid	air	100-300	[103]
Cu@Ag	$Cu(CO_2CH_3)_2$	PVP	EG	co-reduction/ one-pot	$AgNO_3$	EG	Ar	32-48	[104]
Cu@Ag	$CuCl_2$	PVP	$NaBH_4$ trisodium citrate	co-reduction/ one-pot	$AgNO_3$	$NaBH_4$ trisodium citrate	Ar	~25	[105]
Cu@Ag	$Cu(OAc)_2$	PVP	EG	co-reduction/ one-pot	$AgNO_3$	EG	N_2	~81	[101]
Cu@Ag	$CuSO_4$	PVA	$NaBH_4$ ascorbic acid	co-reduction/ one-pot	$[Ag(NH_3)_2]^+$	$NaBH_4$ ascorbic acid	air	32-40	[106]
Cu@Ag	$CuSO_4$	PVP CTAB	NaH_2PO_2	co-reduction/ one-pot	$AgNO_3$	NaH_2PO_2	air	1100-1700	[107]
Cu@Ag	$CuSO_4$	none	$NaBH_4$	co-reduction/ one-pot	$AgNO_3$	$NaBH_4$	air	~17	[108]
Cu@Ag	$CuSO_4$	gelatin	$Na_2S_2O_4$	co-reduction/ one-pot	$[Ag(NH_3)_2]^+$	$Na_2S_2O_4$	air	~15	[109]
Cu@Ag	$CuSO_4$	β-CDs	ascorbic acid	co-reduction/ one-pot	$[Ag(NH_3)_2]^+$	ascorbic acid	air	100-150	[110]
Cu@Ag NWs	$Cu(NO_3)_2$	EDA	glucose	co-reduction/ one-pot	$AgNO_3$	ascorbic acid	air	~245	[113]
Cu@Ag	Cu NWs (commercial)	none	none	co-reduction/ one-pot	$AgNO_3$	ascorbic acid	air	~92	[114]
Cu@Ag	$Cu(NO_3)_2$	PAANa	N_2H_4	transmetalation	$AgNO_3$	none	air	40	[43]
Cu@Ag	$Cu(NO_3)_2$	PAANa	SFS	transmetalation	$[Ag(NH_3)_2]^+$	none	N_2	~913	[50]
Cu@Ag	$CuSO_4$	PVP	EG NaH_2PO_2	transmetalation	$[Ag(NH_3)_2]^+$	none	air	30-80	[119]
Cu@Ag	$CuSO_4$	PVP	N_2H_4	transmetalation	$AgNO_3$	none	air	~5000	[120]
Cu@Ag	$Cu(NO_3)_2$	MEEAA	N_2H_4	transmetalation	$AgNO_3$	none	Ar	~10.2	[121]
Cu@Ag	$CuSO_4$	CTAB	$NaBH_4$	transmetalation	$AgNO_3$	none	N_2	3-55	[122]
Cu@Ag	$CuSO_4$	PVP	$NaBH_4$	transmetalation	$AgNO_3$ $[Ag(NH_3)_2]^+$	none	N_2	~10	[123]

		core synthesis			shell synthesis					
chemical	Cu@Ag	$Cu(CO_2CH_3)_2$	OAm	OAm	transmetalation	$AgNO_3$	none	Ar	13.5	[124]
	Cu@Au	Cu NWs (commercial)	none	none	co-reduction/ one-pot	$HAuCl_4$	ascorbic acid	air	~93	[114]
	Cu@Au	$CuCl_2$	Brij30	$NaBH_4$	co-reduction/ one-pot	$HAuCl_4$	$NaBH_4$	Ar	15-25	[115]
	Cu@Au	$Cu(AOT)_2$	NaAOT	N_2H_4	co-reduction/ one-pot	$HAuCl_4$	N_2H_4	N_2	~8	[56]
	Cu@Pt	Cu NWs (commercial)	none	none	co-reduction/ one-pot	K_2PtCl_6	ascorbic acid	air	~183	[114]
	Ni@Ag	$NiCl_2$	none	N_2H_4 EG	co-reduction/ one-pot	$AgNO_3$	N_2H_4 EG	air	15.4-19.7	[112]
	Ni@Ag	$NiCl_2$	PEI PVP	SFS	co-reduction/ one-pot	$[Ag(NH_3)_2]^+$	SFS N_2H_4	air	~7	[51]
	Ni@Ag	$NiCl_2$	CTAB	N_2H_4	co-reduction/ one-pot	$[Ag(NH_3)_2]^+$	N_2H_4	air	16	[52]
	Ni@Ag	$Ni(CH_3COO)_2$	SDS	N_2H_4	co-reduction/ one-pot transmetalation	$AgNO_3$	tartaric acid	air	107.7-121.5	[53]
	Ni@Ag	$Ni(CH_3COO)_2$	PAANa	$NaBH_4$	transmetalation	$[Ag(NH_3)_2]^+$	none	air	~280	[54] [116] [117]
	Ni@Ag	$NiSO_4$	CMCNa	$NaBH_4$	transmetalation	$AgNO_3$	none	air	220	[118]
	Ni@Au	$NiCl_2$	Brij30	$NaBH_4$	transmetalation	$HAuCl_4$	none	Ar	15-30	[55]
	Ni@Pt	$NiCl_2$	tetraoctylammonium bromide	triethyl lithium borohydride	co-reduction/ one-pot	$PtCl_2$	triethyl lithium borohydride	air	4-8	[111]
physical	Cu@Ag	$Cu(acac)_2$	PVA	none	e-beam irradiation	$AgNO_3$	none	air	~200	[125]
chemical and physical	Cu@Ag	$Cu(OAc)_2$	PVP	glycerol	microwave polyol process transmetalation	$AgNO_3$	none	air	~90	[93]
	Cu@Ag	$Cu(NO_3)_2$	PVP	glycerol	microwave transmetalation	$AgNO_3$	none	air	40-50	[94]
	Cu@Ag	$Cu(NO_3)_2$	sodium acrylate	sodium acrylate	microwave transmetalation	$AgNO_3$	none	air	~44	[95]
	Cu@Ag	Copper myristate	PVA	none	microwave transmetalation	Silver myristate	none	Ar	12–30	[96]
	Cu@Ag	$CuSO_4$	none	none	sono and electrochemical transmetalation	Ag_2O	none	air	10-8	[87]

Abbreviations: PVP – polyvinylpyrrolidone, EDA – ethylenediamine, EG – ethylene glycol, CTAB – cetyltrimethylammonium bromide, NaAOT – sodium bis(2-ethylhexyl)sulfosuccinate, PAANa – polyacrylic acid sodium salt, SDS – sodium dodecyl sulfate, PEI – polyethyleneimine, β-CDs – β-cyclodextrins, CMCNa – sodium carboxymethyl cellulose, Brij30 – polyoxyethylene lauryl ether, $Cu(acac)_2$ – copper acetylacetonate, $Cu(OAc)_2$ – copper acetate, OAm – oleylamine, SFS – sodium formaldehyde sulfoxylate dihydrate, MEEAA – 2-[2-(2-methoxyethoxy)ethoxy]acetic acid.

3.1. Chemical methods

Chemical methods are based on the formation of both metallic core and shell in solution, by reduction of their precursors. In this section we consider the general chemical approaches for the synthesis of metallic core-shell NPs, with various modifications.

3.1.1. Co-reduction (one-pot) method

At this approach, at the first stage, a non-noble metal precursor of the core particle is reduced with a proper reducing agent, and then the shell precursor is added to the same reaction mixture, in some cases together with an additional amount of a reducer. Such an approach is widely used for the fabrication of Cu@Ag, Ni@Ag and Ni@Pt NPs [51,101,103–112]. An analogous procedure was applied for the synthesis of Cu@Ag, Cu@Au, and Cu@Pt NWs [113,114].

In a typical procedure of one-pot simultaneous reduction [105], a coppers salt, $CuCl_2$, was dissolved in water together with a stabilizing agent, polyvinylpyrrolidone (PVP) while stirring at 100 °C under N_2 atmosphere. Then the solution containing the reducing agents, sodium borohydride and trisodium citrate, was added, and the reaction mixture was stirred again at 100 °C. Afterward, the resultant solution was cooled slowly under N_2 atmosphere, and silver nitrate (Ag:Cu atomic ratio 1:8) was added while stirring for 10 min at 100 °C.

The core-shell NPs can also be prepared by the water-in-oil microemulsion method [52,55,56,115]. For example, the Cu cores were prepared by reduction of copper ions within the aqueous phase of reverse water-in-isooctane microemulsion stabilized by AOT, with the use of hydrazine as a reducing agent, and then Au shell was formed after addition of an aqueous solution of $HAuCl_4$ [56].

One-pot method is widely used and, in some cases, leads to obtaining NPs and NWs with well-defined core-shell structures [53,110,113,114]. For example, Fig. 1 shows the SEM and TEM images of Cu@Ag and Cu@Au NWs obtained by reductive deposition of Ag and Au shells onto preformed Cu NWs [114]. The distinct core-shell morphology is clearly seen.

Nevertheless, this method has some disadvantages, which may affect its efficiency in the preparation of high-quality core-shell NPs. First, the addition of a shell precursor into the reaction mixture containing a reducing agent can lead to the reduction of this precursor with the formation of dispersed NPs of the noble metals such as Ag and Au in the liquid phase, and not on the surface of the core particle. A preferential process is determined by the electromotive force, which is the difference in reduction potentials (ΔE^0) of metal ions and the reducing agent.

For example, ΔE^0 values for the pairs Ni/Ag and Cu/Ag are 1.05 and 0.46 V, respectively, while for hydrazine/Ag or $NaBH_4$/Ag they are 1.96 V and 2.04 V, respectively. Therefore, the preferred reaction will be electron transfer to the ions of noble metals from the reducing agent and not from the surface atoms of core nanoparticles, at least in the case of strong reducing agents. It means that NPs of noble metals will be formed in the volume, and shell deposition is suppressed. Therefore, frequently observed two peaks in plasmon spectra and XRD patterns of synthesized NPs are not the correct indications of core-shell structure, since it can indicate a mixture of two types of NPs, not core-shell structure. Secondly, very small NPs of a noble metal can be formed and grow on the surface of larger core particles as centers of nucleation that will lead to the formation of core-shell structures with uniform core particles coated with a shell of more or less densely packed NPs of a noble metal. It seems that this is exactly the situation depicted in Fig. 2, where small Ag NPs are clearly seen on the surface of Cu and Ni core particles [53,110]. In addition, as to TEM images, it is often difficult to distinguish the core

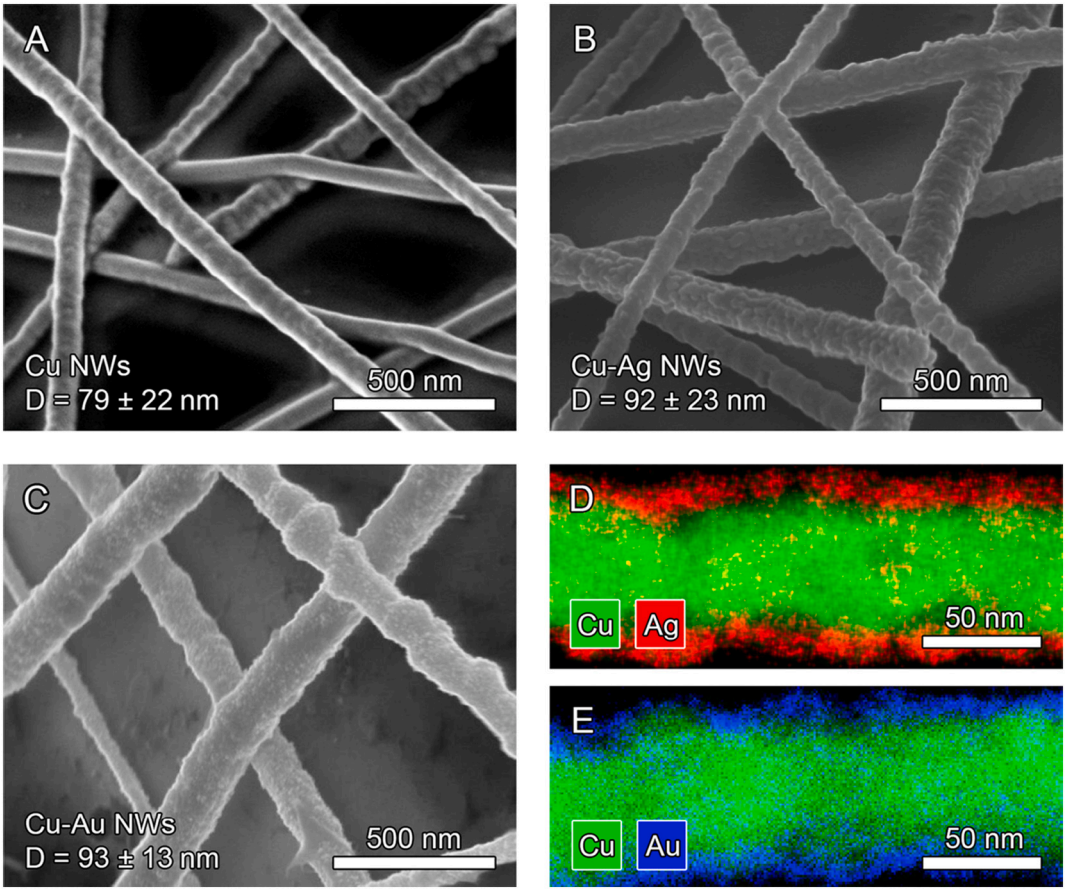

Fig. 1. SEM images of Cu NWs (A), Cu@Ag NWs (B) and Cu@Au NWs (C) and TEM-EDS images of Cu@Ag (D) and Cu@Au (E) NWs. [114]. Reprinted with permission of The American Chemical Society.

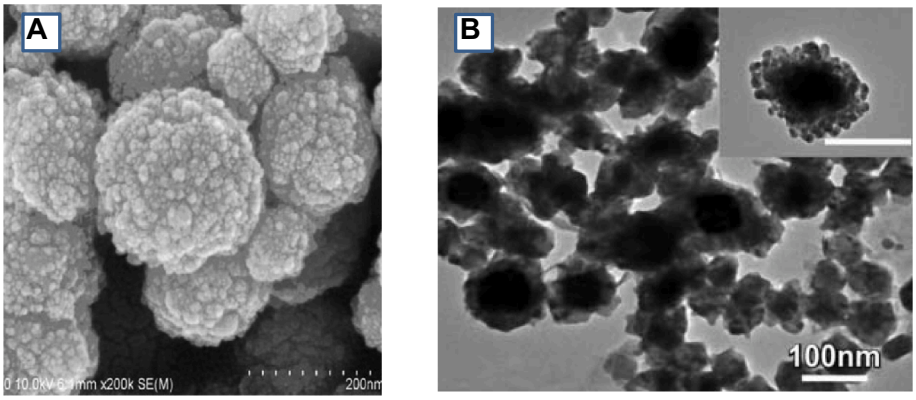

Fig. 2. (A) Field Emission–SEM image of Cu@Ag NPs obtained by sequential reduction of ammonia complexes of copper and silver [110] (Reprinted with permission of Elsevier) and (B) TEM image of Ni@Ag NPs obtained by reduction of $AgNO_3$ in the dispersion of Ni powder [53] (Reprinted with permission of Taylor and Francis).

and shell since the difference in the contrast between metals such as Cu and Ag is too low when Ag serves as a shell, especially in the case of thin shells [43,96].

3.1.2. Transmetalation method

Transmetalation, or galvanic displacement, is apparently the most effective wet chemistry method for fabrication of metallic core-shell NPs. By this process, as schematically presented in Fig. 3, the surface of the preformed core functions (and is sacrificed) as a reducing agent for the second metal with higher reduction potential, thus resulting in the formation of solely metal shell on the surface of the metallic core. Due to a large difference between the reduction potentials of non-noble metals such as Cu an Ni, and noble metals, such as Ag and Au, this method is especially effective in the preparation of relevant core-shell NPs.

An important challenge while using this method is the presence of the rest of the reducing agent in the reaction mixture after the core NPs synthesis. To address this issue, several approaches are usually applied: (i) using stoichiometric amount or a minor deficiency of the reducing agent while synthesizing the core NP; (ii) thorough rinsing of the prepared core NPs by sequential rinsing-centrifugation steps before shell deposition; (iii) removing the excess of the reducing agent by its decomposition or by addition of a proper chemical reagent prior to the addition of a shell precursor, and (iv) obtaining core particles by decomposition of a core metal precursor without using an external reducing agent.

The stoichiometric amount and minor deficiency of a reducing agent relative to precursor were effectively used for producing core Ni NPs (complexes of Ni^{2+} with ammonia or aminomethyl propanol as metal precursors and $NaBH_4$ as a reducing agent) [54,116–118].

Thorough washing by sequential rinsing-centrifugation steps was used, for example, to obtain a dispersion of core Cu NPs free of a reducing agent, formaldehyde sulfoxylate [50], and hypophosphite [119], and for obtaining the dispersion of Cu NWs free of hydrazine [120]. Ni core NPs free of hydrazine were also obtained by washing before Ag coating [53].

Removal of the excess of the reducing agent by adding a proper chemical reagent was for the first time successfully performed by treatment of aqueous dispersion of Cu NPs containing an excess of hydrazine, with acetaldehyde [40,43]. Following coating resulted in obtaining a dispersion of Cu@Ag NPs, which did not contain Ag NPs (Fig. 4). The same approach was reported in [121]. These NPs demonstrate characteristic XRD patterns and plasmon spectra. As seen in Fig. 4c, EDS analysis in STEM mode by scanning an individual Cu@Ag NP along its diameter indicates the presence of the two metals in a single particle: a typical silver profile shows higher intensity at the edges than at the center, while the same scan for copper shows a complementary profile with higher intensity at the center [43]. For obtaining Cu@Ag NPs, H_2SO_4 was also used to remove excess of a reducing agent, sodium borohydride [122,123].

Ni@Au NPs were produced by the spontaneous decomposition of an excess of $NaBH_4$ after core synthesis in reverse microemulsion followed by transmetalation reaction after the addition of chloroauric acid [55].

In addition to the above methods, core NPs free of reducing agents can be produced by the decomposition of a metal salt or coordination complexes. For example, Cu@Ag NPs were obtained by thermal decomposition of copper acetylacetonate in oleylamine, and Ag shells were formed on the surface of as-synthesized Cu NPs by the transmetalation method [124,125]. The EDS scanning along the diameter of these NPs clearly indicates the core-shell structure [125].

3.2. Combination of physical and chemical methods

Physical methods may be especially useful for large-scale fabrication of NPs since they do not require large amounts of chemical reagents, which very often are not eco-friendly. However, to the best of our knowledge, these methods are practically not in use, with the exception of e-beam irradiation. By using this method, high-quality Cu@Ag NPs were obtained with copper acetylacetonate and silver nitrate as core and shell precursors, respectively (their mixture in aqueous solution was

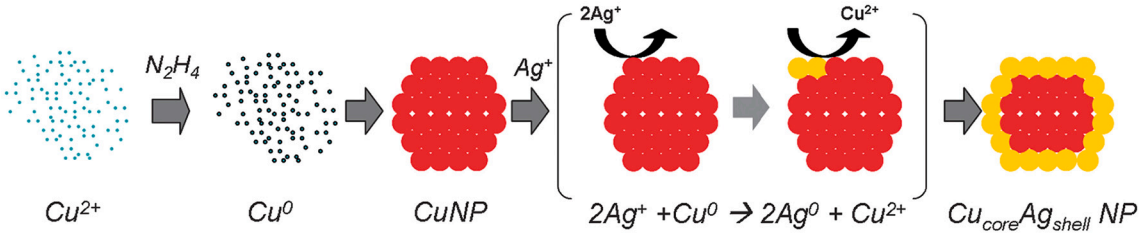

Fig. 3. Schematic illustration of a single Cu NP synthesis and the formation of Ag shell by the transmetalation reaction. The surface copper atoms serve as reducing agents for the silver ions [43]. Reprinted with permission of The Royal Society of Chemistry.

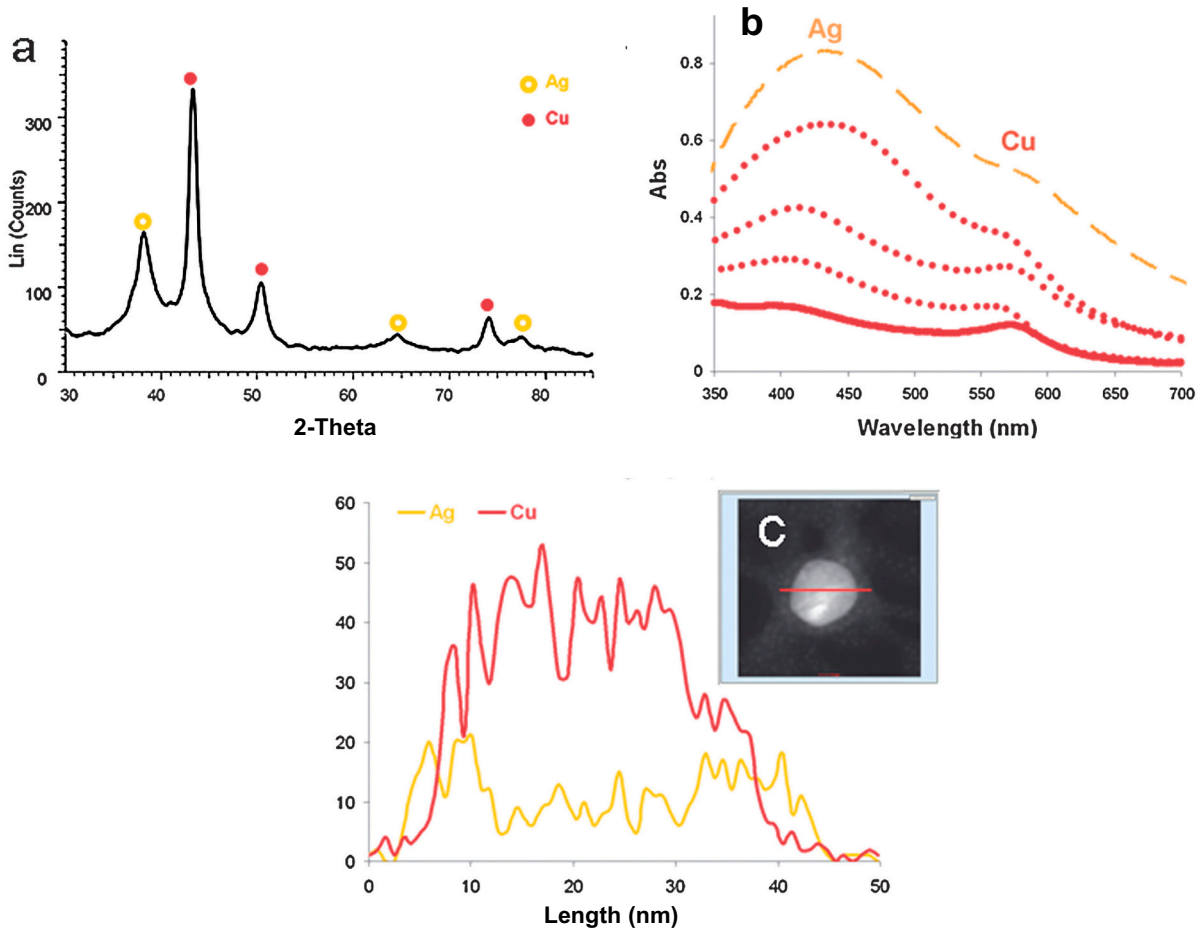

Fig. 4. (a) XRD pattern of a dried dispersion of Cu@Ag NPs at room temperature with characteristic d-spacings of copper (2.089, 1.809 and 1.279 Å) and silver (2.355, 1.444 and 1.231 Å). (b) Absorption spectra of diluted dispersions of Cu@Ag NPs at increasing silver to copper atomic ratio (0, solid line and 0.02 to 1.0, dotted lines to dashed line). (c) STEM image of a 40 nm particle. (d) Copper and silver elemental profile along the particle diameter according to EDS analysis [43]. Reprinted with permission of The Royal Society of Chemistry.

irradiated with e-beam energy of 0.3 MeV) [126]. More success was achieved while combining physical and chemical methods. For example, Cu@Ag NPs were successfully synthesized by heating a mixture of copper nitrate and sodium acrylate in a sealed glass vial to 160 °C in a microwave reactor followed by a transmetalation reaction with silver nitrate [95]. An analogous approach was applied for the synthesis of Cu@Ag NPs in glycerol. After microwave irradiation of the solution of a copper salt, silver acetate [93] or silver nitrate [94] solutions were added to coat these NPs with a silver layer [93,94]. In another approach, Cu@Ag NPs were prepared by ultrasound-assisted electrochemical method (obtaining Cu NPs by sonoelectrolysis of copper sulfate, their thorough washing and drying, followed by transmetalation reaction in solution of a silver salt) [87]. One more method of Cu@Ag NPs fabrication is pulse Cu wire evaporation resulting in obtaining core Cu NPs, followed by transmetalation reaction in $AgNO_3$ solution in ethylene glycol (Fig. 5) [127]. This method can be applicable for the large-scale production of various core-shell NPs.

4. Oxidation stability of core-shell NPs

As written above, oxidation stability of metallic NPs is a crucial property for their practical applications in various areas, such as catalysis, magnetic and optical devices, conductive coatings and printed electronics. In the latter case, the function of the noble metal shell is to protect the core metal from oxidation at ambient conditions and at elevated temperatures, which are usually required at the post-printing sintering step to provide high electrical conductivity of metallic coatings. In addition, to be of practical and commercial importance, the shelf-life of liquid inks or powders containing core-shell NPs should be sufficiently long.

One of the important parameters affecting the oxidation stability of core-shell NPs, especially at elevated temperatures, is the thickness of the metallic shell, which is usually tuned by changing the molar ratio of the core and shell precursors.

As was demonstrated in several reports, for small Cu@Ag NPs (~10–50 nm), a molar copper to silver ratio of less than 5:1 (at the stage of shell formation) is required to ensure the oxidation stability [43,96,121,124,125,128], while for larger NPs with diameter ≥ 100 nm, the effective protection of Cu core can be achieved at Cu:Ag ratio of ≥10:1 [121,127].

The oxidation stability of core-shell NPs is usually evaluated by TG/DTA, XRD, and, in the case of thin metallic shells, by XPS methods.

4.1. Stability at ambient conditions

The long-term stability in air at room temperature, from several weeks to several months, was demonstrated for Cu@Ag NPs synthesized by various methods, with average sizes in the range of 10 to 50 nm [43,94,96,105,119,121,122,124,125,128,129] as well as for submicron [50,102,127] and even micron-sized Cu@Ag particles [50,130]. Fig. 6 presents the pattern of the XPS peaks of 2p Cu for a powder of Cu@Ag NPs with an average diameter of 40 nm and shell thickness in the range

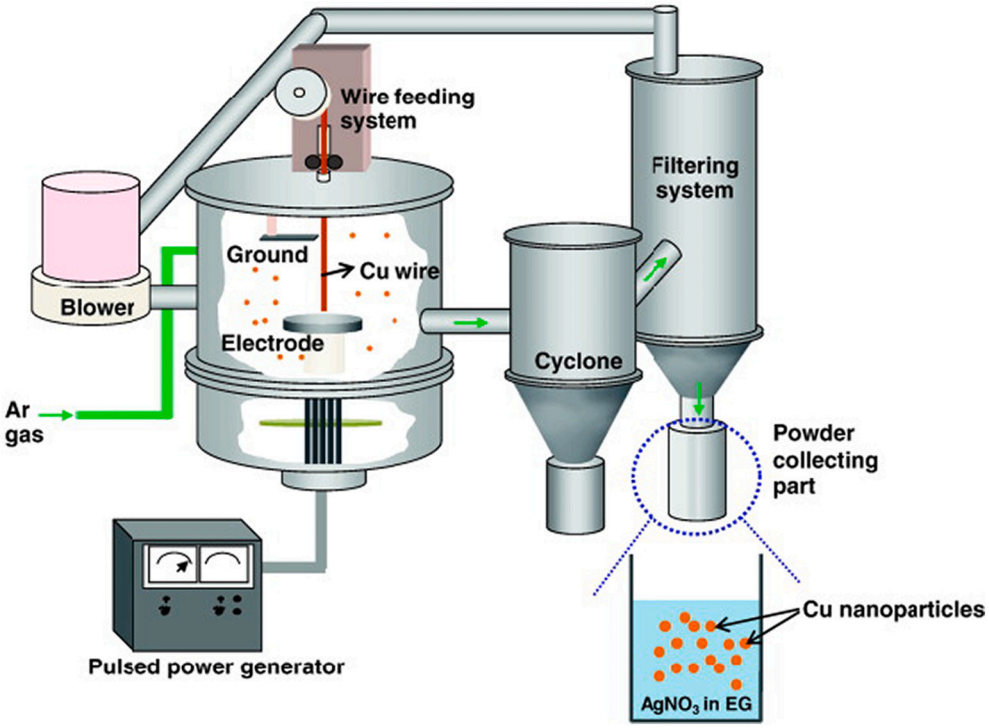

Fig. 5. Scheme of fabrication of Cu@Ag NPs by pulse Cu wire evaporation followed by transmetalation [127]. Reprinted with permission of Elsevier.

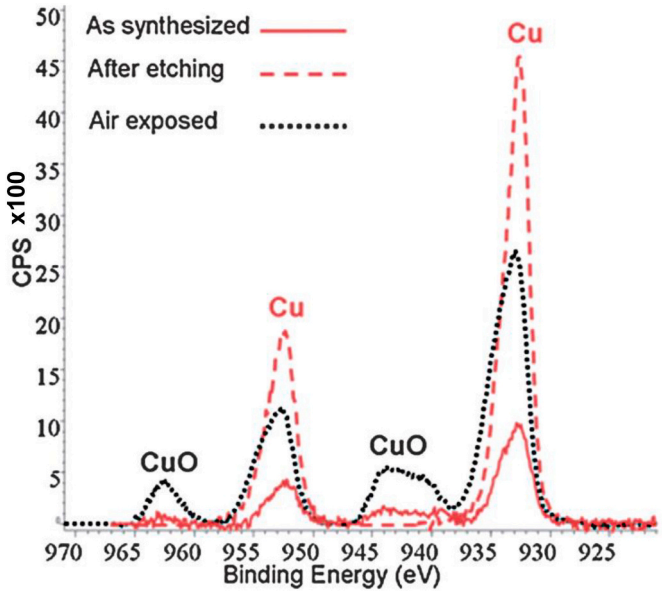

Fig. 6. XPS analysis of a dried powder of Cu@Ag NPs NPs (solid line), after Ar etching (dashed line) and after exposure to air (dotted line) [43]. Reprinted with permission of The Royal Society of Chemistry.

of 2–5 nm (Fig. 4c) [43]. This pattern for as- synthesized NPs is characterized by the peaks typical of both metals and does not show any indications for the presence of copper oxides. However, etching of the surface layer with an ionized Ar beam results in a drastic increase in the intensity of Cu bands, due to the removal of the Ag shell. After exposing the etched sample to air, the intensity of peaks corresponding to metallic Cu decreased, and new peaks characteristic of CuO appeared. These results clearly indicate that the Cu core NPs are indeed protected from oxidation by the Ag shell, and the stability is preserved during at least several months [40,43].

As for Ni@Ag NPs, the core Ni, according to the reduction potential, is much easily oxidizes compared to core Cu. Therefore, during the transmetalation process at ambient conditions, a certain fraction of nickel atoms in the core material undergoes oxidation. Nevertheless, storage of aqueous dispersion of Ni@Ag NPs with average sizes of 50 and 210 nm for six months, lead to a very minor increase in the Ni oxide content, if at all [116].

4.2. Thermal stability

In numerous cases, the core-shell NPs and NWs possess stability to oxidation after being heated to elevated temperatures. It should be noted that the threshold temperatures at which the oxidation starts are in a wide range of ~120–300 °C [43,50,96,105,114,119,121,122,127–130] and depend on particle size and shell thickness (the latter are not indicated in many reports). For example, copper oxides were not detected while heating small Cu@Ag NPs with an average diameter of 8 nm and polydisperse NPs with diameters in the range of 12–30 nm [96] to 146.6 °C and 118 °C, respectively [129]. Oxidation threshold 125 °C was found for Cu@Ag NPs with size 10 nm and shell thickness 1–2 nm [121], while for 17 nm particles the characteristic peaks of copper oxides appear at 250 °C [128]. For 50 nm NPs this threshold was found to be 156 °C [119]. Cu@Ag NPs with wide size distribution (3–50 nm) were stable at heating up to 130 °C [122]. Submicron [50,103,127] and micron-sized Cu@Ag [107,130] particles were found to be stable to oxidation at heating up to 200–250 °C and 200–400 °C, respectively.

Cu@Ag NWs also display stability to heating. For example, NWs with a length of 28 μm, a diameter of 79 nm and shell thickness of 5 nm are stable at heating to 160 °C [114], while NWs with a length of 5–10 nm and diameter of 15–200 nm were stable while heated to ~230 °C [120].

As to Ni@Ag NPs, the stability to oxidation while heating up to 280 °C and 300 °C, respectively, was demonstrated for small NPs composed of 6.2 nm Ni core and 0.85 nm Ag shell [51] and 8 nm Ni core and 6 nm Ag shell [52]. Larger NPs with 70–80 nm and 250–280 nm cores and 20 nm and 40 nm shells, respectively, were stable after heating

to 350 °C [54].

The instability of core-shell NPs to heating is usually related to destroying the protective shell. Enhanced self-diffusion of surface atoms, which intensifies with an increase in temperature makes the metal NPs much "softer" compared to large particles [131,132]. This also results in a drastic decrease in the melting point of metal NPs and enables their sintering (welding) at relatively low temperatures [131,133]. Since in most cases the thickness of the shell is low, not more than several nanometers, their physicochemical properties may be analogous to those of NPs, and the mobility of shell atoms increases. In addition, in the case of Cu@Ag NPs, such a "dewetting" process can occur as a result of very low mutual solubility between Ag and Cu, resulting from considerable lattice mismatch [119,121]. As a result, agglomerates of Ag atoms are formed and grow on the core surface which becomes easily accessible for oxygen. Such a mechanism of high-temperature destabilization of Cu@Ag NPs is discussed in a number of reports [43,105,119,122,124,127,128]. An analogous process was shown to take place during long storage (12 months of aging) of the NPs dispersion [124]. A schematic illustration of the process and HR-SEM images of the Cu@Ag NPs coated on glass slides by inkjet printing and heated under N_2 at various temperatures are presented in Fig. 7 [43].

It was also demonstrated that at a much higher temperature, 500 °C, some core-shell particles can be broken exposing the inside of the particle, and EDS line scan, as well as point analysis, indicate that fragments attached to the inner surface of the broken particle are composed of Ag [130].

5. Conductive coatings

5.1. Formulation of metallic inks

The typical ink for conductive coatings and printing contains a conductive material (e.g. metallic core@shell NPs), aqueous or organic liquid vehicle, and various additives that enable optimal printing performance and good quality of the printed patterns [134,135]. The main and most important component of such nanoink is the conductive material. Generally, the higher the NPs loading in the ink, the higher the conductivity of coating or printed patterns that can be achieved, since the more concentrated NPs suspension provides more metal in a given printing pass and a higher number of contact points and percolation paths between NPs in the metallic film. The loading of metal NPs in conductive nanoink formulation is typically in the range of 20–80 wt% [136]. The inks based on core@shell NPs with concentrations of Cu@Ag NPs of 25–30% [50,119–122,125] and Ni@Ag of 15–25% [54,117,118,137] and 60% [53] were fabricated so far. Such concentrated nanoinks are usually formed by a few-steps process. The dispersion of synthesized NPs can be concentrated by centrifugation/precipitation followed by redispersion in a proper amount of liquid vehicle such as toluene [125], propylene glycol [50], ethylene glycol [50,119,122], water [54,117,118] ethylacetate–terpineol [138], acetone, n-butanol, and propylene glycol monobutyl ether [121] to obtain the highly concentrated nanoink. An important parameter is the remaining non-conductive materials after the evaporation of the solvent. Therefore, it is essential to perform the synthesis at the lowest possible ratio of dispersants to metal particles. To minimize the amount of remaining dispersion agent and other non-conductive additives, the

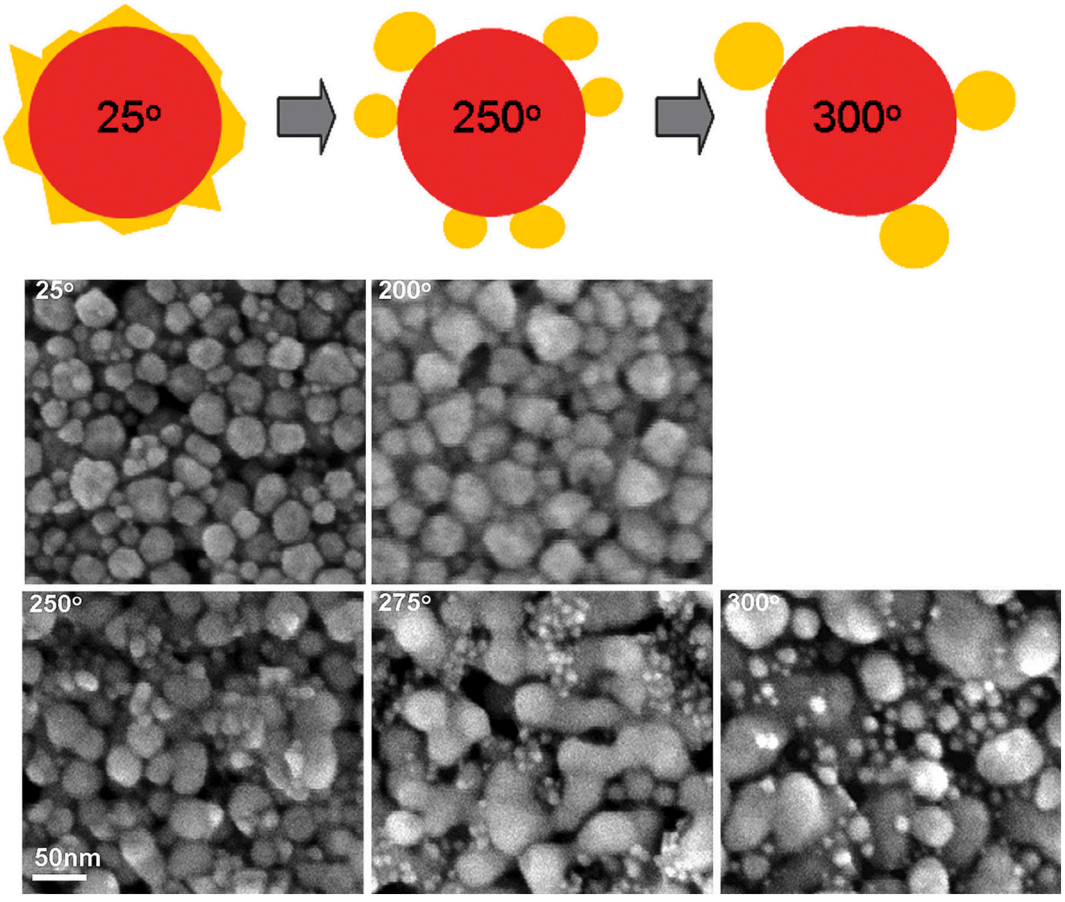

Fig. 7. Schematic illustration of the growing silver crystallites on the copper core (upper image) and HR-SEM images of the Cu@Ag NPs inkjet printed on glass slides and heated under N_2 at various temperatures [43]. Reprinted with permission of The Royal Society of Chemistry.

excess of the stabilizing agent and other organic additives is usually removed by washing the precipitated core@shell NPs with a proper solvent, such as diethylhydroxylamine [114], ethanol [53,103,104,114,122,130], hexane [125], or water [50,53,54,103,116–118,122,138]. In a number of the processes of nanoink preparation, after removing (washing out) of the supernatant, the drying of solid precipitates in air [121,138], vacuum [53,103,104,119], or in desiccator [130] was carried out. The properties of the metallic ink should be also optimized to provide a good coating/printing process, optimal wetting and adhesion to the substrate, which are required to obtain uniform conductive films. For example, to obtain high-quality coatings, inks containing Ni@Ag NPs, were tailored by adding Surfynol PSA 336 [118] or TEGO WET KL 245 [54,117,137] as wetting agents.

It should be also noted that in addition to the metallic core-shell NPs, the conductive ink contains various additives such as rheology and surface tension modifiers, humectants, binders, and defoamers that enable optimal conditions for the fabrication of conductive patterns or coatings [2,5]. For example, in the case of inkjet printing, the optimal ink viscosity and surface tension should be in the range of 1–15 cP and 25–35 mN/m, respectively [135]. Furthermore, the size of the NPs should be tailored according to the printing and wet-deposition methods. For example, it should be less than 0.01–0.1 of the diameter of the printhead orifice (20–50 μm) of inkjet printer to avoid its blockage [2,5].

5.2. Formation of conductive coatings and printed patterns

In general, to obtain metallic conductive patterns, two steps are usually required: (1) deposition of the metallic ink by coating or printing on a proper substrate and (2) sintering of the metallic particles within the pattern, that often enables removing organic additives and the stabilizing agent, which, being adsorbed on the surface of particles, prevents inter-particle contacts. Sintering results in desorption and/or decomposition of the insulating organic materials, and a tightly packed or welded metallic layer with high conductivity is formed [2,5,7]. This can be achieved by various techniques: heating at elevated temperature, applying intense light pulse, microwave radiation, plasma, high electrical field, and action of chemical agents [2,5,7]. As a characteristic of conductive coatings, sheet resistance measured by a four-points probe is usually used (results presented as Ω/sq. or Ω/□). To obtain the resistivity of the conductive layer, the sheet resistance should be multiplied by the film thickness.

The deposition of Cu@Ag NPs-based conductive inks was performed by a variety of methods, including roller pen [122], spin coating [125], bar coating [50,114], inkjet [25,43] or screen printing [104,114,135]. Inks based on Ni@Ag NPs were deposited on various substrates by bar coating [54,117,118,137] and screen printing [53,117] techniques.

The most common method of sintering the films formed by core-shell NPs is their heating to elevated temperatures. It is based on a two-step process. In the first step, thermal decomposition and evaporation of organic additives occur, that leads to the formation of necks and inter-particle connections. In the second step, grains of core-shell NPs grow as the result of inter-particle atomic diffusion, which provides conductivity resembling the properties of a bulk metal [25,139]. It should be noted that although most common, thermal sintering is limited to applications utilizing heat resistant substrates, such as glass, ceramics or polyimide, and is not applicable to paper and heat-sensitive polymeric substrates, such as PEN and PET, which are often used in flexible electronics.

The final conductivity/resistivity of thermally sintered coatings or patterns formed by inks composed of core@shell NPs depends on a number of factors, such as size of nanoparticles, molar core-to-shell ratio, the type and concentration of organic additives (e.g. polymeric stabilizers), but the most important is the sintering temperature. In many cases, the reported electrical characteristics of conductive coatings are difficult to compare, since the resistivity should be calculated from the measured sheet resistance only if the film thickness is known. Therefore, it is more desirable to report the resistivity values or at least the % of bulk resistivity of the pure metal. In the following section, we will describe, in more details, the characteristics of conductive coatings formed by two types of particles, Cu@Ag and Ni@Ag.

5.2.1. Cu@Ag particles

In the case of Cu@Ag NPs, the sintering temperature, at which highly conductive coatings are formed, is usually in the range of 15 0–350 °C. For example, the resistivity of patterns that were inkjet printed onto glass slides decreased from $3{\cdot}10^4$ μΩ·cm to 11 μΩ·cm (which is only 7 times greater than that of bulk copper) with increasing sintering temperature from 150 °C to 300 °C [43]. Such ink was shown to be suitable for the fabrication of RFID antenna as shown in Fig. 8 [40]. Similarly, a decrease in resistance from 2.84 Ω/□ (56.73 μΩ·cm) to 0.60 Ω/□ (12.0 μΩ·cm) with an increase in the sintering temperature from 200 °C to 350 °C was observed [125]. The lowest resistivity is very similar to the resistivity of commercial Ag conductive inks (2.34–15.9 μΩ·cm) [31], although the Ag content in Cu@Ag NPs was only about 20%.

Pen-drawn electrical circuit with resistivity of 13.8 μΩ·cm formed by Cu@Ag NPs ink sintered at 150 °C for 1 h in N_2 was shown to be effective in ordinary small bulb operation (Fig. 9) [122].

Film formed by Cu@Ag nanoink on a polymeric substrate, polyimide, by screen printing and sintered at 200 °C, had a resistivity 8.2 μΩ·cm that is only about 5 times higher than the resistivity of bulk copper [127].

In addition to NPs, submicron and micron-sized Cu@Ag particles were tested as the conductive components of inks and pastes. For example, a paste containing 100–1000 nm particles and screen printed onto a glass substrate, formed conductive films with a resistivity of 255 and 142.5 μΩ·cm after sintering at 250 and 350 °C, respectively [138]. It was also found that the addition of carboxylic acids to the ink based on submicron Cu@Ag particles stabilized by polyacrylate leads to improved conductivity of films deposited on a glass substrate and heated at 250 °C (11.7 and 6.9 μΩ·cm for films formed by ink without and with oleic acid, respectively). The function of the acid was supposed to be a destabilization of a layer of polyacrylate causing its detachment from the particles surface [140].

As an alternative method to thermal sintering, photonic sintering was applied. The advantages of this method in comparison to thermal sintering are a very short exposure time and a high power that can be used to control the temperature that reduces the risk of heat-sensitive

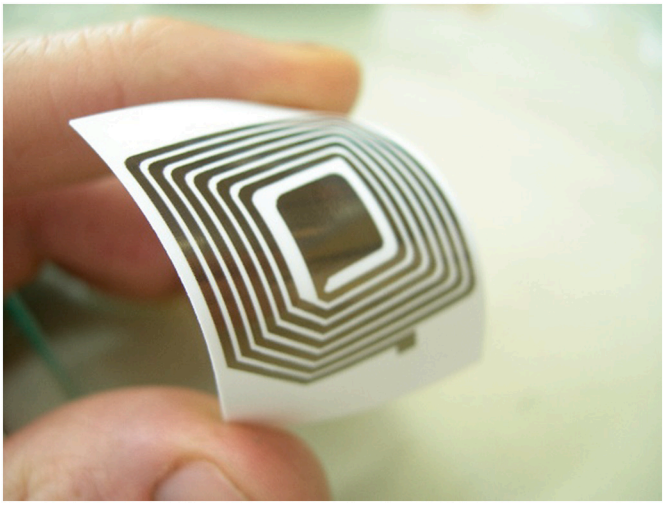

Fig. 8. A flexible RFID antenna inkjet printed on photopaper using ink containing 25 wt% Cu@Ag [40]. Reprinted with permission of MDPI.

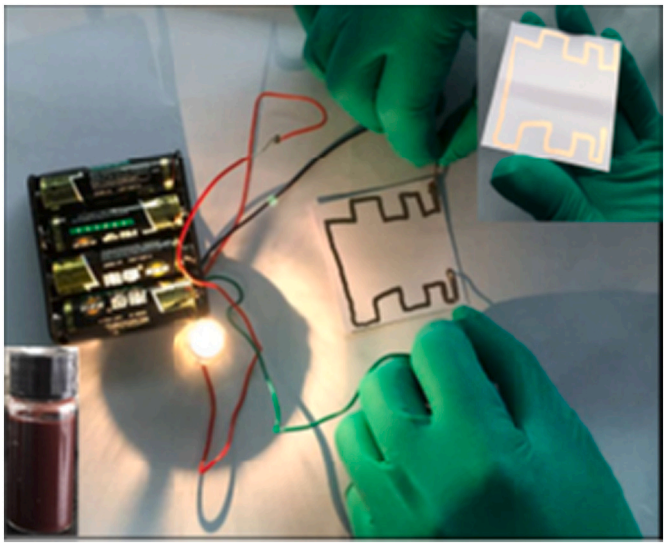

Fig. 9. The conductive circuit drawn on photo paper by using a roller pen and sintered at 150 °C for 1 h in N_2 atmosphere and ordinary small bulb operation. Inset: high-resolution of the conductive pattern [122]. Reprinted with permission of Springer.

substrates destruction. An intense pulse light was used for sintering of films formed by Cu@Ag NPs, and the obtained resistivity was as low as 15.18 μΩ·cm, nine times higher than the resistivity of bulk copper [141]. The studies on the fabrication of electrodes for OPV devices by using intense pulsed light, demonstrated that the copper-to-silver molar ratio strongly affects the film resistance, which increases with the increase of copper concentration, that can be related to the increase in content of copper oxides [104].

One more method for obtaining tightly packed conductive Cu@Ag films (64.24 μΩ·cm) was pressing the as-prepared NPs under an axial pressure of 20 MPa [142].

Highly conductive patterns were obtained by using a hybrid ink composed of a mixture of micron-sized Cu@Ag particles and individual Ag NPs with an average size of 60 nm [107]. Patterns drawn on a photo-paper by a brush pen and sintered at 160 °C for 2 h had resistivity 5 μΩ·cm that is only 3 times higher than the silver bulk resistivity.

Typical changes of the deposited films morphologies and the electrical resistivities after sintering at various temperatures are presented in Fig. 10. As seen, an increase in temperature results in the formation of a film with more tight packing of Cu@Ag NPs and its distinct welding at 300 and 350 °C [125].

In addition to experimental works, theoretical studies on the sintering process of core-shell NPs were performed. The multiple sintering model of Cu@Ag NPs with molecular dynamics was used to present the dependency of the sintering process of NPs on their size, porosity, crystallinity, and applied temperature, as well as mechanical and thermodynamic properties of the sintered structures [139]. The effect of shell thickness of Cu@Ag NPs on their sintering process was also investigated by using the atomistic sintering simulation method. It was found that thinner shells prevent the contribution of the plastic deformation mechanism to sintering, and the proportion of amorphous Ag atoms at the sintering neck increases. Furthermore, at higher sintering temperature the diffusion of Cu atoms near the core-shell interface can occur, especially for the Cu@Ag with a thin shell [143].

In regard to NWs, it was shown that Cu@Ag, Cu@Au, and Cu@Pt NWs rod-coated onto glass slides were conductive immediately after coating and after following heating at 160 °C in a dry oven for 24 h [114]. Incorporation of Cu@Ag NWs into polycaprolactone with a melting point in the range of 59–64 °C resulted in the formation of filaments suitable for 3D printing of conductive patterns with a resistivity of $2{\cdot}10^3$ μΩ·cm, without any post-printing treatment [113]. Fig. 11 shows a 3D printed inductive charging coil, powering a LED using a wireless charging dock.

5.2.2. Ni@Ag particles

A conductive paste containing 65 wt% of Ni@Ag NPs with an average size 104 nm was screen printed on a polycrystalline silicon substrate, and the obtained film had a sheet resistance of 11 mΩ/□ after sintering at 650 °C. This value is superior to this of the Ni paste, and close to that of the Ag pastes [53]. The obtained results can be explained by improved oxidation stability of Ni@Ag NPs and their tighter packing in the sintered film compared to the film formed by Ni paste, in which a number of defects and voids are clearly seen in SEM images.

The conductivity of Ni@Ag NPs ink coatings (average sizes of NPs

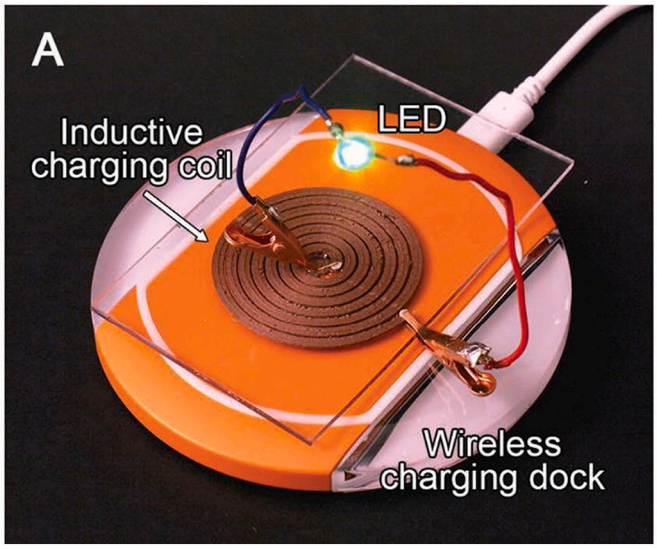

Fig. 11. Demonstration showing how the Cu@Ag NW filament can be used for 3D printing of an inductive charging coil to wireless power of LED [113]. Reprinted with permission of Wiley-VCH.

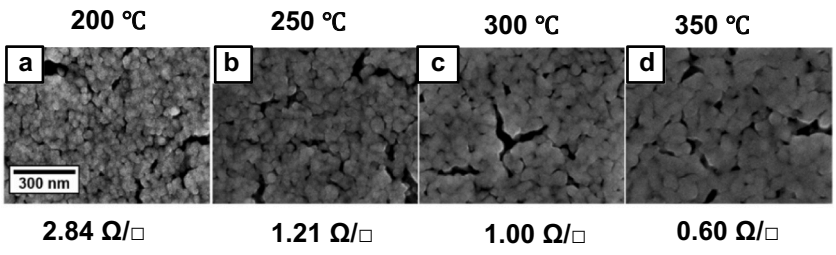

Fig. 10. SEM images of surface morphology and sheet resistance of Cu@Ag films spin coated onto glass slides and sintered at various temperatures [125]. Reprinted with modifications and permission of IOP Publishing.

obtained in the processes with excess and deficiency of a reducing agent were 80 and 280 nm, respectively) on glass substrate after the sintering at various temperatures, was analyzed [54]. Sintering of coatings obtained with larger NPs at 350 °C resulted in lower resistivity compared to smaller nanoparticles, and the lowest value was found to be 63 μΩ·cm. This finding was explained as a result of a higher atomic percentage of metallic unoxidized nickel in the dispersion of larger than smaller Ni@Ag NPs [116]. Fig. 12 shows the morphologies of coatings after sintering at various temperatures for 30 min. The obtained images clearly indicate the formation of a uniform layer composed of tightly packed and welded Ni@Ag NPs being sintered at 350 °C [54].

To improve the conductivity, the use of Ni@Ag ink with the bimodal size distribution was evaluated. It was hypothesized that smaller particles will fill the voids between larger particles thus providing more tightly packed films. By using ink containing Ni@Ag NPs with average sizes 70 and 250 nm and 1:1 mass ratio, metallic films were formed on glass slides by bar coating and screen printing, and such films that were sintered at 300 and 350 °C, respectively, were found to have a conductivity that is 80% higher compared with films formed by mono-sized Ni@Ag NPs [117].

The ink formulation containing three types of Ni@Ag NPs (Fig. 13) demonstrated very high efficiency in obtaining conductive coatings [137]. It was found that the conductivity of films on a glass substrate obtained by bar coating with the use of optimal ink composition (mass ratio of 110, 220, and 420 nm particles 1:1.5:0.5) and sintered at 300 °C was much higher compared to that of coatings formed by monodisperse inks and is $9.9 \cdot 10^6$ S/m, i.e. as high as ~69% of bulk nickel.

The same idea, to improve NPs packing in the deposited metallic film, was realized by the formulation of conductive ink containing Ni@Ag NPs with an average size of 220 nm and doped with smaller Ag NPs (30 nm) [118]. Such ink containing 1 wt% of Ag NPs and coated on glass slides provided film conductivity of $6.1 \cdot 10^6$ S/m (35% of the bulk Ni conductivity) after sintering at temperature as low as 150 °C. The similar conductivity was obtained while using ink containing 0.5 wt% of Ag NPs, but the sintering temperature was higher, 200 °C.

The possibility to obtain conductive patterns at low heating temperatures makes such inks suitable for printing on heat-sensitive plastic and paper substrates.

6. Outlook

The main reason for using core-shell NPs as a functional component of conductive inks is to replace an expensive silver, which is used currently in most conductive metallic inks in printed electronics. Among the non-noble metals, copper possesses high electrical conductivity, which is only ~6% lower than conductivity of silver. Another highly conductive metal, aluminum, undergoes very rapid oxidation with the formation of a dense oxide layer that makes it very difficult to handle as core material for fabrication of core-shell NPs. Nickel, the conductivity of which is ~23% of silver conductivity can be also considered as an attractive material, for producing core-shell nanoparticles.

As follows from the above review, there is remarkable scientific and technological progress in the fabrication of oxidation-resistive metallic core-shell materials, especially Cu@Ag NPs. However, there are several issues to be addressed before the effective integration of such materials into large-scale industrially printed 2D and 3D electronic devices, with an estimated market of more than $73 billion in 2027 [144]. One of the main challenges is the development of efficient low-cost methods for the

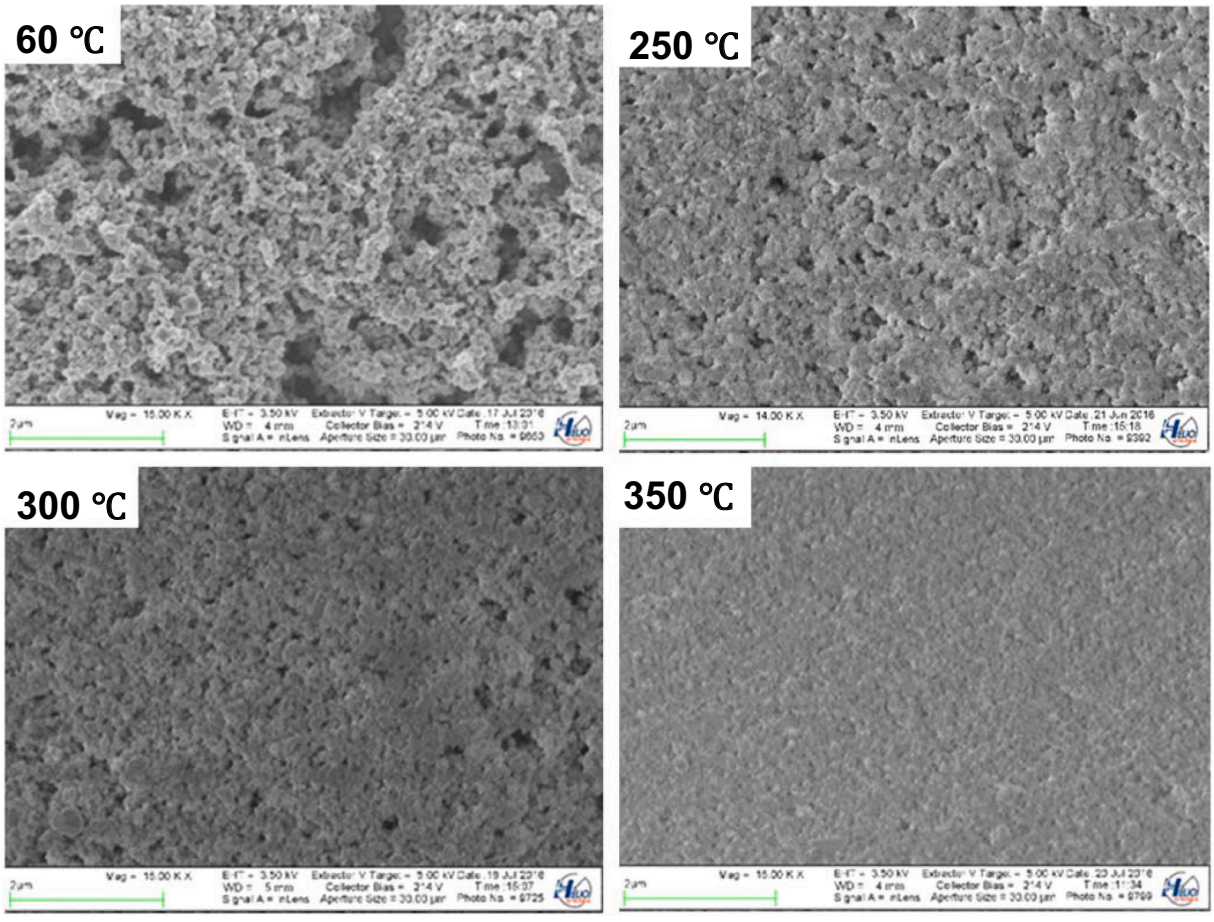

Fig. 12. SEM images of ink coatings composed of Ni@Ag NPs with an average size 280 nm after sintering at various temperatures for 30 min [54]. Reprinted with permission of IOP Publishing.

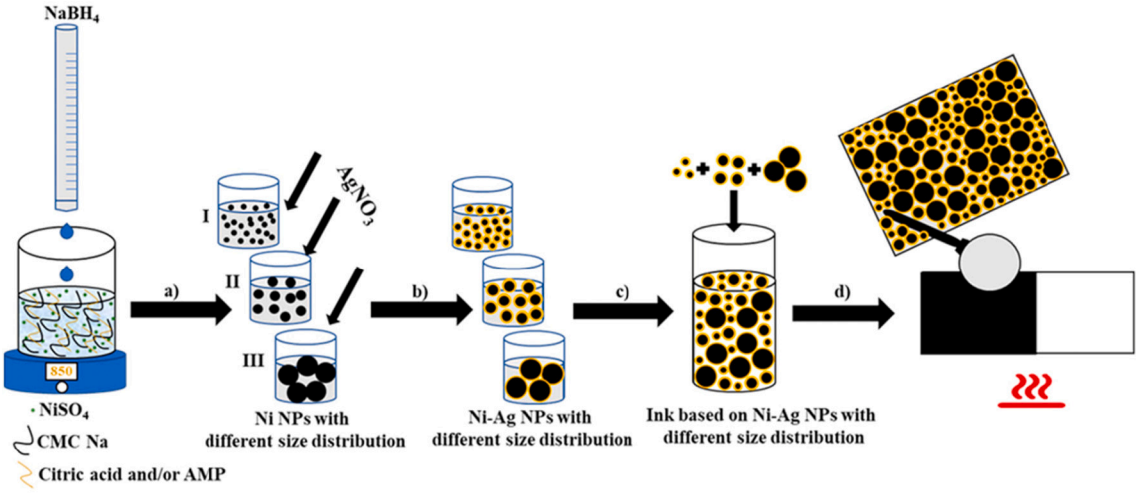

Fig. 13. Scheme of preparation of the conductive coatings based on Ni@Ag NPs: (a) optimization of the process of synthesis of Ni NPs with different size distributions; (b) formation of Ni@Ag NPs by transmetalation method; (c) preparation of ink containing Ni@Ag NPs with various sizes; (d) fabrication of conductive metallic films by bar coating [137]. Reprinted with permission of MDPI.

fabrication of the core-shell NPs. It seems that eco-friendly physical methods, which do not require large amounts of chemical reagents are the most promising. Of great importance is also developing new and simple methods for post-printing treatment, which will be compatible with substrates, which are sensitive to elevated temperatures and which enable preserving the original chemical composition of the cores and shells.

We expect that the progress in producing and utilization of core-shell particles, methods of coating/printing and post-printing treatment will lead to low-cost and large-scale fabrication of highly effective 2D and 3D electronic devices, conductive components of which are based on metallic core-shell materials.

Declaration of Competing Interest

The authors declare that they have no known competing financial interests or personal relationships that could have appeared to influence the work reported in this paper.

Acknowledgements

This project was partially supported by the European Union's Horizon 2020 research and innovation programme under the Marie Skłodowska-Curie grant agreement No 955612 and by the National Polish Centre, Poland, grant number 2020/39/D/ST5/01937.

References

[1] Abbel R, Meinders ER. Printing technologies for nanomaterials. In: Kamyshny A, Magdassi S, editors. Nanomaterials for 2D and 3D printing. Weinheim, Germany: Wiley-VCH; 2017. p. 1–26.
[2] Kamyshny A, Magdassi S. Matallic nanoinks for inkjet printing of conductive 2D and 3D structures. In: Kamyshny A, Magdassi S, editors. Nanomaterials for 2D and 3D printing. Weinheim, Germany: Wiley-VCH; 2017. p. 119–60.
[3] Li J, Lemme MC, Östlung M. Graphene- and 2D material-based thin-film printing. In: Kamyshny A, Magdassi S, editors. Nanomaterials for 2D and 3D printing. Weinheim, Germany: Wiley-VCH; 2017. p. 161–81.
[4] Jeong S, Moon J. Printable semiconducting/dielectric materials for printed electronics. In: Kamyshny A, Magdassi S, editors. Nanomaterials for 2D and 3D printing. Weinheim, Germany: Wiley-VCH; 2017. p. 213–27.
[5] Kamyshny A, Magdassi S. Conductive nanomaterials for 2D and 3D printed flexible electronics. Chem Rev 2019;48:1712–40.
[6] Huang Q, Zhu Y. Printing conductive nanomaterials for flexible and stretchable electronics: a review of materials, processes, and applications. Adv Mater Technol 2019;4:1800546.
[7] Reinhold I. Inkjet printing of functional materials and post-processing. In: Kamyshny A, Magdassi S, editors. Nanomaterials for 2D and 3D printing. Weinheim, Germany: Wiley-VCH; 2017. p. 27–49.
[8] Perelaer I, Schubert US. Inkjet printing of interconnects and contacts based on inorganic nanoparticles for printed electronic applications. In: Korvink JP, Smith PJ, Shin D-Y, editors. Inkjet-based micromanufacturing. Weinheim, Germany: Wiley-VCH; 2012. p. 347–64.
[9] Cummins G, Desmulliez MPY. Inkjet printing of conductive materials: a review. Circuit Word 2012;38:193–213.
[10] An BW, Kim K, Lee H, Kim S-Y, Shim Y, Lee D-Y, et al. High-resolution printing of 3D structures using an electrohydrodynamic inkjet with multiple functional inks. Adv Mater 2015;27:4322–8.
[11] Hong K, Kim SH, Mahajan A, Frisbie CD. Aerosol jet printed p- and n-type electrolyte-gated transistors with a variety of electrode materials: exploring practical routes to printed electronics. ACS Appl Mater Interfaces 2014;6:18704–11.
[12] Cao C, Andrews JB, Kumar A, Franklin AD. Improving contact interfaces in fully printed carbon nanotube thin-film transistors. ACS Nano 2016;10:5221–9.
[13] Wang S, Liu N, Yang C, Liu W, Su J, Li L, et al. Fully screen printed highly conductive electrodes on various flexible substrates for asymmetric supercapacitors. RSC Adv 2015;5:85799–805.
[14] Antuña-Jiménez D, González-García MB, Hernández-Santos D, Fanjul-Bolado P. Screen-printed electrodes modified with metal nanoparticles for small molecule sensing. Biosensors 2020;10:10020009.
[15] Hösel M, Søndergaard RR, Angmo D, Krebs FC. Comparison of fast roll-to-roll flexographic, inkjet, flatbed, and rotary screen printing of metal back electrodes for polymer solar cells. Adv Eng Mater 2013;15:995–1001.
[16] Secor EB, Lim S, Zhang H, Frisbie CD, Francis LF, Hersam MC. Gravure printing of graphene for large-area flexible electronics. Adv Mater 2014;26:4533–8.
[17] Shacham-Diamand Y, Sverdlov E, Friedberg S, Yaverboim A. Electroless plating and printing technologies. In: Kamyshny A, Magdassi S, editors. Nanomaterials for 2D and 3D printing. Weinheim, Germany: Wiley-VCH; 2017. p. 51–67.
[18] Wang X, Zhi L, Müllen K. Transparent, conductive graphene electrodes for dye-sensitized solar cells. Nano Lett 2008;8:323–7.
[19] Kumar D, Stoichkov V, Ghosh S, Smith GC, Kettle J. Mixed-dimension silver nanowires for solution-processed, flexible, transparent and conducting electrodes with improved optical and physical properties. Flex Print Electron 2017;2:015005.
[20] Dan B, Irvin GC, Pasquali M. Continuous and scalable fabrication of transparent conducting carbon nanotube films. ACS Nano 2009;3:835–43.
[21] Leem D-S, Edwards A, Faist M, Nelson J, Bradley DDC, de Mello JC. Efficient organic solar cells with solution-processed silver nanowire electrodes. Adv Mater 2011;23:4371–5.
[22] Hecht DS, Heintz AM, Lee R, Hu L, Moore B, Cucksey C, et al. High conductivity transparent carbon nanotube films deposited from superacid. Nanotechnol. 2011;22:075201.
[23] Pei S, Du J, Zeng Y, Liu C, Cheng H-M. The fabrication of a carbon nanotube transparent conductive film by electrophoretic deposition and hot-pressing transfer. Nanotechnol. 2009;20:235707.
[24] Yin S, Sun S, Salim T, Wu S, Huang X, He Q, et al. Organic photovoltaic devices using highly flexible reduced graphene oxide films as transparent electrodes. ACS Nano 2010;4:5263–8.
[25] Kamyshny A, Magdassi S. Conductive nanomaterials for printed electronics. Small 2014;10:3515–35.
[26] McCoul D, Hu W, Gao M, Mehta V, Pei Q. Recent advances in stretchable and transparent electronic materials. Adv Electron Mater 2016;2:1500407.
[27] Araki T, Mandamparambil R, Jiu J, Sekitani T, Suganuma K. Application of printed silver nanowires based on laser-induced forward transfer. In:

Kamyshny A, Magdassi S, editors. Nanomaterials for 2D and 3D printing. Weinheim, Germany: Wiley-VCH; 2017. p. 265–73.
[28] Harris KD, Elias AL, Chung H-J. Flexible electronics under strain: a review of mechanical characterization and durability enhancement strategies. J Mater Sci 2016;51:2771–805.
[29] Brannelly NT, Killard AJ. Inkjet-printable nanomaterials and nanocomposites for sensor fabrication. In: Kamyshny A, Magdassi S, editors. Nanomaterials for 2D and 3D printing. Weinheim, Germany: Wiley-VCH; 2017. p. 293–316.
[30] Singh M, Haverinen HM, Dhagat P, Jabbour GE. Inkjet printing – process and its applications. Adv Mater 2010;22:673–85.
[31] Kamyshny A, Steinke J, Magdassi S. Metal-based inkjet inks for printed electronics. Open Appl Phys J 2011;4:19–36.
[32] Farraj Y, Smooha A, Kamyshny A, Magdassi S. Plasma-induced decomposition of copper complex ink for the formation of highly conductive copper tracks on heat-sensitive substrates. ACS Appl Mater Interfaces 2017;9:8766–73.
[33] Farraj Y, Grouchko M, Magdassi S. Self-reduction of a copper complex MOD ink for inkjet printing conductive patterns on plastics. Chem Commun 2015;51:1587–90.
[34] Rosen YS, Yakushenko A, Offenhausser A, Magdassi S. Self-reducing copper precursor inks and photonic additive yield conductive patterns under intense pulsed light. ACS Omega 2017;2:573–81.
[35] Layani M, Kamyshny A, Magdassi S. Transparent conductors composed of nanomaterials. Nanoscale 2014;6:5581–91.
[36] Rathmell AR, Wiley BJ. The synthesis and coating of long, thin copper nanowires to make flexible, transparent conducting films on plastic substrates. Adv Mater 2011;23:4798–803.
[37] Perelaer J, Abbel R, Wünscher S, Jani R, van Lammeren T, Schubert US. Roll-to-roll compatible sintering of inkjet printed features by photonic and microwave exposure: from non-conductive ink to 40% bulk silver conductivity in less than 15 seconds. Adv Mater 2012;24:2620–5.
[38] Perelaer J, Jani R, Grouchko M, Kamyshny A, Magdassi S, Schubert US. Plasma and microwave flash sintering of a tailored silver nanoparticle ink, yielding 60% bulk conductivity on cost-effective polymer foil. Adv Mater 2012;24:3993–8.
[39] Grouchko M, Kamyshny A, Ben-Sami K, Magdassi S. Synthesis of copper nanoparticles catalyzed by pre=formed silver nanoparticles. J Nanopart Res 2009;11:713–6.
[40] Magdassi S, Grouchko M, Kamyshny A. Copper nanoparticles for printed electronics: routes towards achieving oxidation stability. Materials 2010;3:4626–38.
[41] Campbell T, Kalia RK, Nakano A, Vashishta P. Dynamics of oxidation of aluminum nanoclusters using variable charge molecular-dynamics simulations on parallel computers. Phys Rev Lett 1999;82:4866–9.
[42] Foley TJ, Johnson CE, Higa KT. Inhibition of oxide formation on aluminum nanoparticles by transition metal coating. Chem Mater 2005;17:4086–91.
[43] Grouchko M, Kamyshny A, Madassi S. Formation of air-stable copper-silver core-shell nanoparticles for inkjet printing. J Mater Chem 2009;19:3057–62.
[44] Jeong S, Lee SH, Jo Y, Lee SS, Seo Y-H, Ahn BW, et al. Air-stable, surface-oxide free Cu nanoparticles for highly conductive Cu ink and their application to printed graphene transistors. J Mater Chem 2013;1:2704–10.
[45] Kwon J, Park S, Haque MM, Kim Y-S, Lee CS. Study of sintering behavior of vapor forms of 1-octanethiol coated copper nanoparticles for application in ink-jet technology. J Nanosci Nanotechnol 2012;12:3434–7.
[46] Song X, Sun S, Zhang W, Yin Z. A method for the synthesis of spherical copper nanoparticles in the organic phase. J Colloid Interface Sci 2004;273:463–9.
[47] Liu X, Wang D, Li Y. Synthesis and catalytic properties of bimetallic nanomaterials with various architectures. Nano Today 2012;7:448–66.
[48] Boote BW, Hongsik B, Kim J-H. Silver-gold bimetallic nanoparticles and their application as optical materials. J Nanosci Nanotechnol 2014;14:1563–77.
[49] Zaleska-Medynska A, Marchelek M, Diak M, Grabowska E. Nobel metal-based bimetallic nanoparticles: the effect of the structure on the optical, catalytic and photocatalytic properties. Adv Colloid Interface Sci 2016;229:80–107.
[50] Pajor-Świerzy A, Farraj Y, Kamyshny A, Magdassi S. Air stable copper-silver core-shell submicron particles: synthesis and conductive ink formulation. Colloids Surf A 2017;521:272–80.
[51] Lee C-C, Chen D-H. Large-scale synthesis of Ni-Ag core-shell nanoparticles with magnetic, optical and anti-oxidation properties. Nanotechnol. 2006;17:3094–9.
[52] Thu NNA, Park JG, Kim S-H. Synthesis of Ni-Ag core-shell nanoparticles by polyol process and microemulsion process. Bull Korean Chem Soc 2013;34:2865–70.
[53] Jing JJ, Xie J, Chen GY, Li WH, Zhang MM. Preparation of nickel-silver core-shell nanoparticles by liquid-phase reduction for use in conductive paste. J Exp Nanosci 2015;10:1347–56.
[54] Pajor-Świerzy A, Socha R, Pawlowski R, Warszyński P, Szczepanowicz K. Application of metallic inks based on nickel-silver core-shell nanoparticles for fabrication of conductive films. Nanotechnol. 2019;30:225301.
[55] Chen D, Li J, Shi C, Du X, Zhao N, Sheng J, et al. Properties of core-shell Ni-Au nanoparticles synthesized through a redox-transmetalation method in reverse microemulsion. Chem Mater 2007;19:3399–405.
[56] Larios E, Molina Z, Maldonado A, Tanori J. Synthesis and characterization of bimetallic copper-gold nanoparticles. J Dispers Sci Technol 2012;33:719–23.
[57] Schmid G. Metals. In: Klabunde KJ, editor. Nanoscale materials in chemistry. New York: John Wiley & Sons; 2001. p. 15–59.
[58] Tretyakov YD, Lukashin AV, Eliseev AA. Synthesis of functional nanocomposites based on solid-phase nanoreactors. Russ Chem Rev 2004;73:899–921.
[59] Teranishi T. Metallic colloids. In: Somasundaram P, editor. Encyclopedia of surface and colloid science. Boca Raton: Taylor & Francis; 2012. p. 3662–74.
[60] Pitkethly MJ. Nanomaterials – the driving force. Mater Today 2004;7:20–9.
[61] Kotov YA. Electric explosion of wires as a method for preparation of nanopowders. J Nanopart Res 2003;5:539–50.
[62] Kamyshny A, Magdassi S. Aqueous dispersions of metallic nanoparticles. Preparation, stabilization, and application. In: Starov V, editor. Nanoscience: colloidal and interfacial aspects. Boca Raton-London-New York: CRC Press; 2010. p. 747–78.
[63] Fiévet F. Polyol process. In: Schick MJ, Hubbard AT, editors. Fine particles: Synthesis, characterization, and mechanism of growth. New York-Basel: Marcel Dekker; 2000. p. 460–96.
[64] Toshima N. Reactions in homogeneous solutions. In: Schick MJ, Hubbard AT, editors. Fine particles: synthesis, characterization, and mechanism of growth. New York-Basel: Marcel Dekker; 2000. p. 430–59.
[65] Dupont J, Fonseca GS, Umpierre AP, Fichtner PFP, Teixeira SR. Transition-metal nanoparticles in imidazolium ionic liquids: recyclable catalysts for biphasic hydrogenation reactions. J Am Chem Soc 2002;124:4228–9.
[66] Jung I, Jo YH, Kim I, Lee HM. A simple process for synthesis of Ag nanoparticles and sintering of conductive ink for use in printed electronics. J Electron Mater 2012;41:115–21.
[67] Philippot K, Chaudret B. Organometallic approach to the synthesis and surface reactivity of noble metal nanoparticles. C R Chim 2003;6:1019–34.
[68] Green M. Organometallic based strategies for metal nanocrystal synthesis. Chem Commun 2005:3002–11.
[69] Chen W-D, Lin Y-H, Chang C-P, Sung Y, Liu Y-M, Ger M-D. Fabrication of high-resolution conductive line via inkjet printing of nano-palladium catalyst onto PET substrate. Surf Coat Technol 2011;205:4750–6.
[70] Liz-Marzán LN. Nanomaterials: formation and color. Mater Today 2004;7:26–31.
[71] Sun Y, Xia Y. Gold and silver nanoparticles: a class of chromophores with colors tunable in the range from 400 to 750 nm. Analyst 2003;128:686–91.
[72] Goia DV, Matijević E. Preparation of monodispersed metal particles. New J Chem 1998;22:1203–15.
[73] Murphy CJ, Sau TK, Gole AM, Orendorff CJ, Gao J, Gou L, et al. Anisotropic metal nanoparticles: synthesis, assembly, and optical applications. J Phys Chem B 2005;109:13857–70.
[74] Antelman MS. Chemical electrode potentials. New York-London, USA: Plenum Press; 1982.
[75] Couto GG, Klein JJ, Schreiner WH, Mosca DH, de Oliveira AJA, Zarbin AJG. Nickel nanoparticles obtained by a modified polyol process: synthesis, characterization, and magnetic properties. J Colloid Interface Sci 2007;311:461–8.
[76] Bai L, Yuan F, Tang Q. Synthesis of nickel nanoparticles with uniform size via a modified hydrazine reduction route. Mater Lett 2008;62:2267–70.
[77] Eluri R, Paul B. Synthesis of nickel nanoparticles by hydrazine reduction: mechanistic study and continuous flow synthesis. J Nanopart Res 2012;14:800.
[78] Singh K, Kate KH, Chilukuri VVS, Khanna PK. Glycerol mediated low temperature synthesis of nickel nanoparticles by solution reduction method. J Nanosci Nanotechnol 2011;11:5131–6.
[79] Jo YH, Jung I, Choi CS, Kim I, Lee HM. Synthesis and characterization of low temperature Sn nanoparticles for the fabrication of highly conductive ink. Nanotechnol. 2011;22:225701.
[80] Shen W, Zhang X, Huang Q, Xu Q, Song W. Preparation of solid silver nanoparticles for inkjet printed flexible electronics with high conductivity. Nanoscale 2014;6:1622–8.
[81] Lee Y, Choi JR, Lee KJ, Stott NE, Kim D. Large-scale synthesis of copper nanoparticles by chemically controlled reduction for applications of inkjet-printed electronics. Nanotechnol. 2008;19:415604.
[82] Tang XF, Yang ZG, Wang WJ. A simple way of preparing high-concentration and high-purity nano copper colloid for conductive ink in inkjet printing technology. Colloids Surf A 2010;360:99–104.
[83] Starowicz M, Stypuła B, Banaś J. Electrochemical synthesis of silver nanoparticles. Electrochem Commun 2006;8:227–30.
[84] Cheon J, Lee J, Kim J. Inkjet printing using copper nanoparticles synthesized by electrolysis. Thin Solid Films 2012;520:2639–43.
[85] Dhas NA, Raj CP, Gedanken A. Synthesis, characterization, and properties of metallic copper nanoparticles. Chem Mater 1998;10:1446–52.
[86] Yang GW, Li H. Sonochemical synthesis of highly monodispersed and size controllable Ag nanoparticles in ethanol solution. Mater Lett 2008;62:2189–91.
[87] Mancier V, Rousse-Bertrand C, Dille J, Michel J, Fricoteaux P. Sono and electrochemical synthesis and characterization of copper core-silver shell nanoparticles. Ultrason Sonochem 2010;17:690–6.
[88] Haas I, Shanmugam S, Gedanken A. Pulsred sonoelectrochemical synthesis of size-controlled copper nanoparticles stabilized by poly(N-vinylpyrrolidone). J Phys Chem B 2006;110:16947–52.
[89] Sakamoto M, Fujistuka M, Majima T. Light as a construction tool of metal nanoparticles: synthesis and mechanism. J Photochem Photobiol C 2009;10:33–56.
[90] Kapoor S. Preparation, characterization, and surface modification of silver particles. Langmuir 1998;14:1021–5.
[91] Henglein A, Giersig M. Formation of colloidal silver nanoparticles: capping action of citrate. J Phys Chem B 1999;103:9533–9.
[92] Kapoor S. Effect of ligands on the redox reactions of silver metal clusters. Langmuir 1999;15:4365–9.
[93] Miyakawa M, Hiyoshi N, Nishioka M, Koda H, Sato K, Miyazawa A, et al. Continuous synthesis of Pd@Pt and Cu@Ag core-shell nanoparticles using microwave-assisted core particle formation coupled with galvanic metal displacement. Nanoscale 2014;6:8720–5.

[94] Kheawhom S, Panyarueng P. Synthesis and characterization of copper-silver core-shell nanoparticles by polyol successive reduction process. Mater Res Soc Symp Proc 2014;1630.
[95] Njoki P, Rhoades AE, Barnes JI. Microwave-assisted synthesis of anisotropic copper-silver nanoparticles. Mater Chem Phys 2020;241:122348.
[96] Chen Z, Mochizuki D, Maitani M, Wada Y. Facile synthesis of bimetallic Cu–Ag nanoparticles under microwave irradiation and their oxidation resistance. Nanotechnology 2013;24:265602.
[97] Carrol KJ, Reveles JU, Shiltz MD, Khjanna SN, Carpenter EE. Prepasration of elemental Cu and Ni nanoparticles by the polyol method: an experimental and theoretical approach. J Phys Chem C 2011;115:2656–64.
[98] Tsai C-Y, Chang W-C, Chen G-L, Chung C-H, Liang J-X, Ma WY, et al. A study of the preparation and properties antioxidative copper inks with high electrical conductivity. Nanoscale Res Lett 2015;10:357.
[99] Jeong S, Song HS, Lee WW, Lee SS, Choi Y, Son W, et al. Stable aqueous based Cu nanoparticle ink for printing well-defined highly conductive features on a plastic substrate. Langmuir 2011;27:3144–9.
[100] Mott D, Galkowski J, Wang L, Luo J, Zhong C-J. Synthesis size-controlled and shaped copper nanoparticles. Langmuir 2007;23:5740–5.
[101] Tsui M, Hikino S, Sano Y, Horigome M. Preparation of Cu@Ag core-shell nanoparticles using a top-step polyol process under bubbling N_2 gas. Chem Lett 2009;38:518–9.
[102] Ma Y, Wang L, Ye Q, Qin H, Fu Q. Preparation of Cu@Ag core-shell nanoparticles by $NaBH_4$ combined with NaH_2PO_2 as reductants. Chem Soc Japan 2021;50:184–6.
[103] Yuan Y, Xia H, Chen Y, Xie D. One-step synthesis of oxidation-resistant Cu@Ag core–shell nanoparticles. Micro & Nano Lett 2018;13:171–4.
[104] Yim SJ, Lee JY, Yu J-W. Intense pulsed light sintered core-shell nanoparticles for organic photovoltaic devices. Macromol Res 2019;27:1167–72.
[105] Tsai C-H, Chen S-Y, Song J-M, Chen I-G, Lee H-Y. Thermal stability of Cu@Ag core-shell nanoparticles. Corros Sci 2013;74:123–9.
[106] Trinh CD, Dang DMT, Dang CM. Synthesis core-shell nanoparticles of Cu-Ag for application in electrohydrodynamic printing technique. J Mater Sci Eng 2019;A9(3–4):75–82.
[107] Li W, Wang Y, Wang M, Li W, Tan J, You C, et al. Synthesis of stable $Cu_{core}Ag_{shell}$&Ag particles for direct writing flexible paper-based electronics. RSC Adv 2016;6:62236–43.
[108] Li C, Yao Y. Synthesis of bimetallic core-shell silver-copper nanoparticles decorated on reduced graphene oxide with enhanced electrocatalytic performance. Chem Phys Lett 2020;761:137726.
[109] Jin X, Mao A, Ding M, Ding P, Zhang T, Gu X, et al. A simple route to synthesize Au@Ag core-shell bimetallic nanoiparticles and their surface-enhanced raman scattering proiperties. Appl Spectrosc 2016;70:1692–9.
[110] Zhao J, Zhang D, Zhao J. Fabrication of Cu-Ag core-shell bimetallic superfine powders by eco-friendly reagents and structures characterization. J Solid State Chem 2011;184:2339–44.
[111] Duan D, Liu S, Yang C, Zhang Z, Hao X, Wei G, et al. Electrocatalytic performance of $Ni_{core}@Pt_{shell}$/C core-shell nanoparticles with the Pt nanoshell. Int J Hydrogen Energy 2013;38:14261–8.
[112] Chen D-H, Wang S-R. Protective agent-free synthesis of Ni-Ag core-shell nanoparticles. Mater Chem Phys 2006;100:468–71.
[113] Crus MA, Ye S, Kim MJ, Reyes C, Yang F. Multigram synthesis of Cu-Ag core-shell nanowires enables the production of a highly conductive polymer filament for 3D printing electronics. Part Part Syst Charact 2018;35:1700385.
[114] Stewart IE, Ye S, Chen Z, Flowers PF, Wiley B, J.. Synthesis of Cu-Ag, Cu-Au, and Cu-Pt core-shell nanowires and their use in transparent conducting films. Chem Mater 2015;27:7788–94.
[115] Jing J, Xie J, Chen G, Li W, Zhang M. Syntjhesis of core-shell Cu-Au nanoparticles via a redox-transmetalation method in reverse microemulsion. Adv Mat Res 2013;815:465–8.
[116] Pajor-Świerzy A, Gaweł D, Drzymała E, Socha R, Parlińska-Wojtan, Szczepanowicz K, et al. The optimization of methods of synthesis of nickel-silver core-shell nanoparticles for conductive coatings. Nsnotechnol. 2019;30:015601.
[117] Pajor-Świerzy A, Pawłowski R, Warszynski P, Szczepanowicz K. The conductive properties of ink coating based on Ni-Ag core-shell nanoparticles with the bimodal size distribution. J Mater Sci Mater Electron 2020;31:12991–9.
[118] Pajor-Świerzy A, Szendera F, Pawłowski R, Szczepanowicz K. Nanocomposite inks based on nickel-silver corep-shell and ailver nanoparticles for fabrication conductive coatings at low-temperature sintering. Coll Interfaces 2021;5:15.
[119] Yu X, Li J, Shi T, Cheng C, Liao G, Fan J, et al. A gree approach of synthesizing of Cu-Ag core-shell nanoparticles and their sintering behavior for printed electronics. J Alloys Compd 2017;724:365–72.
[120] Zhao J, Zhang D, Zhang X. Preparation and characterization of copper/silver bimetallic nanowires with core-shell structures. Surf Interface Anal 2015;47:529–34.
[121] Titkov AI, Logutenko OA, Vorobyov AM, Gerasimov EYu, Shundrina IK, Bulina NV, et al. Synthesis of ~10 nm size Cu/Ag core-shell NPs stabilized by an ethoxylated carboxylic acid for conductive ink. Colloids Surf A 2019;577:500–8.
[122] Tan S, Zu X, Yi G, Liu X. Synthesis of highly environmental stable copper-silver core-shell nanoparticles for direct writing flexible electronics. J Mater Sci Mater Electron 2017;28:15899–906.
[123] Huiang Y, Wu F, Zhou Z, Zhou L, Liu H. Fabrication of fully covered Cu-Ag core-shell nanoparticles by compound method and anti-oxidation performance. 2021.
[124] Musikansky A, Nanikashvili P, Grinblat J, Zitoun D. Ag dewetting in Cu@Ag monodisperse core-shell nano/particles. J Phys Chem C 2013;117:3093–100.
[125] Lee C, Kim NR, Koo J, Lee YJ, Lee HM. Cu-Ag core-shell nanoparticles with enhanced oxidation stability for printed electronics. Nanotechnol. 2015;26:455601.
[126] Kang HS, Koo YH, Park HD, Chai G-S, Ryoo SY, Bae HB, et al. Manufacturing method fpr core-shell metal nanoparticle structutre having excellent oxidation stability using Cu@Ag core-shell nanoparticles. J Nanosci Nanotechnol 2015;15:8508–14.
[127] Kim CK, Lee G-J, Lee MK, Rhee CK. A novel method to prepare Cu@Ag core-shell nanoparticles for printed flexible electronics. Powder Technol 2014;263:1–6.
[128] Chee S-S, Lee J-H. Preparation and oxidation behavior of Ag-coated Cu nanoparticles less than 20 nm in size. J Mater Chem C 2014;2:5372–81.
[129] Huang Y, Wu F, Zhou Z, Zhou L, Liu H. Fabrication of fully covered Cu-Ag core-shell nanoparticles be compound methoid and anti-oxidation performance. Nanotechol. 2020;31:175601.
[130] Hai HT, Takamura H, Koike J. Oxidation behavior of Cu-Ag core-shell particles for solar cell applications. J Alloys Compd 2013;564:71–4.
[131] Dick K, Dhanasekaran T, Zhang Z, Meizel D. Size-dependent melting of silica-encapsulated gold nanoparticles. J Am Chem Soc 2002;124:2312–7.
[132] Grouchko M, Roitman P, Zhu X, Popov I, Kamyshny A, Su H, et al. Merging of metal nanoparticles driven by selective wettability of silver nanostructures. Nat Commun 2014;5:2994.
[133] Buffat P, Borel J-P. Size effect on the on the melting temperature of gold particles. Phys Rev A 1976;13:2287–98.
[134] Kamyshny A, Magdassi S. Inkjet ink formulations. In: Korvink JP, Smith PJ, Shin D-Y, editors. Inkjet-based micromanufacturing. Weinheim, Germany: Wiley-VCH; 2012. p. 173–89.
[135] Kamyshny A, Magdassi S. Inkjet printiung. In: Kirk-Othmer enzyclopedia of chemical technology. Weinheim, Germany: Wiley-VCH; 2013. p. 1–21.
[136] Nir MM, Zamir D, Haymov I, Ben-Asher L, Cohen O, Faulkner B, De La Vega F. Electrically conductive inks for inkjet printing. Chemistry of inkjet inks; Magdassi, S. New Jersey, London, Singapore: World Scientific; 2021. p. 225–54.
[137] Pajor- Świerzy A, Staśko D, Pawłowski R, Mordarski G, Kamyshny A, Szczepanowicz K. Polydispersity vs. monodispersity. How the properties of Ni-Ag core-shell nanoparticles affect the conductivity of ink coatings. Materials 2021;14:2304.
[138] Peng Y, Yang C, Chen K, Popuri SR, Lee C-H, Tang B-S. Study on synthesis of ultrtafine Cu-Ag core-shell powders with high electrical conductivity. Appl Surf Sci 2012;263:38–44.
[139] Wang J, Shin S. Sintering of multiple Cu–Ag core–shell nanoparticles and properties of nanoparticle sintered structures. RSC Adv 2017;7:21607.
[140] Pajor-Świerzy A, Farraj Y, Kamyshny A, Magdassi S. Effect of carboxylic acid on conductivity of metallic films formed by inks based on copper@silver core-shell particles. Colloids Surf A 2017;522:320–7.
[141] Park J-W, Jang Y-R, Shin H-S, Kim H-S, Kim JJ. A study on copper-silver core-shell microparticles with silver with silver nanoparticles hybrid paste and its intense pulse light sintering characteristics for high oxidation resistance. 2021.
[142] Shang S, Kunwar A, Wang Y, Qi X, Ma H, Wang Y. Synthesis of Cu@Ag core-shell nanoparticles for characterization of thermal stability and electric resistivity. Appl Phys A 2018;124:492.
[143] Li S, Liu Y, Sun F, Fang H. Multi-particle molecular dynamics simulation: shell thickness effects on sintering process of Cu-Ag core-shell nanoparticles. J Nanopart Res 2021;23:6.
[144] Printed, organic & flexible electronics forecasts, players & opportunities 2017–2027. available from: https://www.idtechex.com/research/reports/printed-organic-and-flexibleelectronics-forecasts-players-and-opportunities-2017-2027-000510.asp; 2021.